JOURNAL OF GEOPHYSICAL RESEARCH, VOL. 117, CXXXXX, doi:10.1029/2011JC007261, 2012

Evaluation and control mechanisms of volume and freshwater export through the Canadian Arctic Archipelago in a high-resolution pan-Arctic ice-ocean model

Timothy McGeehan[1] and Wieslaw Maslowski[1]

Received 4 May 2011; revised 19 December 2011; accepted 9 January 2012; published XX Month 2012.

[1] This study examined the 1979–2004 volume and freshwater fluxes through the Canadian Arctic Archipelago (CAA) and into the Labrador Sea using a high resolution (~9 km) coupled ice-ocean model of the pan-Arctic region to provide a reference, compare with limited observational estimates, and investigate control mechanisms of this exchange. The 26-year mean volume and freshwater fluxes through Nares Strait were 0.77 Sv $\pm$ 0.17 Sv and 10.38 mSv $\pm$ 1.67 mSv respectively, while those through Lancaster Sound amounted to 0.76 Sv $\pm$ 0.12 Sv and 48.45 mSv $\pm$ 7.83 mSv respectively. The 26-year mean volume and freshwater fluxes through Davis Strait were 1.55 Sv $\pm$ 0.29 Sv and 62.66 mSv $\pm$ 11.67 mSv while the modeled Fram Strait branch provided very little (~2%) freshwater into the Labrador Sea compared to the total CAA input. Compared to available observations, the model provides reasonable volume and freshwater fluxes, as well as sea ice thickness and concentration in the CAA. In Nares Strait and Lancaster Sound, volume flux anomalies were controlled by the sea surface height (SSH) gradient anomalies along the straits and freshwater anomalies were highly correlated with the volume anomalies. At least half of the variance in the time series of SSH gradient anomaly was due to SSH anomalies in northern Baffin Bay. The West Greenland Current (WGC) exhibits seasonality, with cross shelf flow (into the Labrador Sea) peaking in January/February/March, while reducing the northward flow across eastern Davis Strait. We hypothesize that the eddy-reduced northward flow of WGC results in the lower volume and SSH in Baffin Bay. This maximizes the SSH gradients between the Arctic Ocean and Baffin Bay, leading to maximum winter volume fluxes through Nares Strait and Lancaster Sound. Model limitations include the insufficient spatial resolution of atmospheric forcing (especially to account for the effects of local topography), the representation of river runoff into Hudson Bay and coastal buoyancy currents, low mobility of modeled ice, and incomplete depiction of ice arching. Many of these issues are expected to be resolved with increased model grid cell resolution, improved sea ice and ocean models and more realistic atmospheric forcing.

Citation: McGeehan, T., and W. Maslowski (2012), Evaluation and control mechanisms of volume and freshwater export through the Canadian Arctic Archipelago in a high-resolution pan-Arctic ice-ocean model, *J. Geophys. Res.*, *117*, CXXXXX, doi:10.1029/2011JC007261.

1. Introduction

[2] The Labrador Sea is one of the few known locations of open ocean deep convection [e.g., *Marshall and Schott*, 1999]. This deep convection is an integral part of the Atlantic meridional overturning circulation (AMOC), a key component of the global climate system often described as the "great ocean conveyor" [*Broecker*, 1991]. Model simulations of AMOC have shown it to be sensitive to freshwater exiting the Arctic Ocean [*Hakkinen*, 1999; *Jungclaus et al.*, 2005; *Hu et al.*, 2008]. In particular, freshwater exiting the Arctic Ocean through the Canadian Arctic Archipelago (CAA) (estimated between 90 and 110 mSv [*Prinsenberg and Hamilton*, 2005]) has been shown to significantly affect modeled AMOC [e.g., *Goosse et al.*, 1997; *Wadley and Bigg*, 2002; *Cheng and Rhines*, 2004; *Komuro and Hasumi*, 2005]. Observational studies [*Belkin et al.*, 1998; *Houghton and Visbeck*, 2002] have also concluded that CAA outflow was most likely a major contributor of low salinity anomalies in the Labrador Sea, such as the "Great Salinity Anomaly" in the 1980s. However, due to coarse spatial resolution in most global ocean models the CAA cannot be accurately

[1]Department of Oceanography, Graduate School of Engineering and Applied Sciences, Naval Postgraduate School, Monterey, California, USA.

represented. In reality the CAA has complex morphology and coastline with numerous narrow and/or shallow sections for which the exact bathymetry is still poorly known despite centuries of exploration. In today's ocean models, the CAA is often represented as a wide single channel, two wide channels, or it is completely closed, thereby distorting or completely preventing the direct flow of low salinity water from the Arctic to Baffin Bay and onwards to the Labrador Sea via this pathway [*Goosse et al.*, 1997; *Wadley and Bigg*, 2002; *Komuro and Hasumi*, 2005; *Koberle and Gerdes*, 2007; *Jahn et al.*, 2010].

[3] The other oceanic freshwater pathway is a much less direct route from the Arctic, transiting Fram Strait and circumnavigating Greenland before arriving in the Labrador Sea. The freshwater signal takes longer to transit to the Labrador Sea and can be diffused and modified significantly along this route [*Williams*, 2004] through mixing with warm and salty Atlantic water in the Nordic and Irminger seas. If a model has an overly wide single channel in lieu of a realistic CAA, too much Arctic freshwater may drain out through that channel, causing an unrealistically large freshwater flux to the Labrador Sea and raising the salinity of the outflow at Fram Strait [*Wadley and Bigg*, 2002]. If a model has the CAA closed altogether, the freshwater must all come through Fram Strait, unrealistically lowering the salinity at Fram Strait. In addition to influencing the freshwater fluxes leaving the Arctic, the width of a modeled CAA channel may also affect the magnitude of Atlantic water input into the Arctic [*Joyce and Proshutinsky*, 2007]. To understand the freshwater input to the Labrador Sea and its impact on deep convection there, both pathways need to be realistically represented in a model.

[4] The explicit modeling of sea ice and ocean as a coupled system responding to atmospheric forcing is also critical to understanding the timing, phase (i.e., solid versus liquid) and location of freshwater export from the Arctic because most of the freshwater flux through Fram Strait is in the form of sea ice, which later undergoes a phase change as it is advected around Greenland. Conversely, the flow through the CAA is predominately in the liquid phase due to the tight constrictions on sea ice drift imposed by the coastline, bathymetry and topography. In addition, the extent of ice cover and location of a marginal ice zone affects momentum transport from the atmosphere and vertical mixing in the ocean.

[5] Prediction of future states of the Arctic and North Atlantic may depend heavily on realistic representation of these seawater phase changes and the CAA pathway. A study by Haak and the MPI Group (cited by *Vellinga et al.* [2008]) suggests that by 2070–2099 freshwater flux through the CAA will increase by 48% whereas the Fram Strait branch will increase only 3% due to the loss of the sea ice component (which currently dominates the Fram Strait outflow). *Koenigk et al.* [2007] came to a similar conclusion, where the relative importance of Fram Strait to the total Arctic freshwater export decreased while the importance of the CAA grew. Such changes contributed to significantly reduced convection in the Labrador Sea and a 6 Sv decrease in their modeled AMOC.

[6] For this study, all calculated fluxes are presented in the form of monthly means and are net fluxes unless otherwise stated. All calculations of freshwater use a reference salinity of 34.8 and liquid equivalent fluxes assume the salinity of sea ice to be 4. Volume fluxes are given in Sv (1 Sv = 1×10^6 m^3 s^{-1}) and freshwater fluxes are given in mSv (1 mSv = 1×10^3 m^3 s^{-1}). Positive flux values are from the Arctic toward the Labrador Sea. Anomalies discussed henceforth are determined by removing the mean annual cycle from the data (i.e., the volume flux anomaly for June 2002 is calculated by removing the 26-year mean June volume flux from the June 2002 volume flux value). Values listed as ± are standard deviations based on the time series of monthly means except where explicitly specified. Total kinetic energy appearing on plots is calculated as TKE = $0.5*(u^2 + v^2)$ and plotted in cm^2 s^{-2}.

[7] Figure 1 denotes several sub- regions that will be discussed in the text and provides a high-resolution image of the CAA bathymetry. This paper starts with a brief description of the model and output used in the next section. Then ocean and sea ice results for the Nares Strait, Lancaster Sound, and CAA are discussed in sections 3, 4, and 5. Exchanges through Davis Strait are presented in section 6 with comparative analyses through Fram Strait and Hudson Bay following in sections 7 and 8. Section 9 includes a discussion of mechanisms controlling fluxes through the CAA (including a description of the dynamics of Baffin Bay). The summary and conclusions are discussed in section 10.

2. Model

[8] This study utilized the Naval Postgraduate School (NPS) Arctic Modeling Effort (NAME) model, a coupled ice-ocean model with horizontal resolution of 1/12° (~9 km). The model domain includes the North Pacific and North Atlantic as well as the Arctic, thus permitting exchanges between the Arctic and sub-Arctic (see *Maslowski et al.* [2008] for the full domain). The grid measures 1280 × 720 points and has 45 vertical fixed-depth layers, with thickness ranging from 5 m near the surface to 300 m at depths. Model bathymetry of the central Arctic is derived from the 2.5 km resolution International Bathymetric Chart of the Arctic Ocean (IBCAO [*Jakobsson et al.*, 2000]) and for the region south of 64°N from ETOPO5 at 5-min resolution. The 9 km horizontal resolution of the domain allows narrow straits and passages to be represented and still have flow while satisfying the no slip boundary condition. Overall, the 9 km resolution allows realistic depiction of the Canadian Arctic Archipelago (Figure 1), and is a major enabler for this study.

[9] The ocean model is a regional application of the Parallel Ocean Program (POP) [*Smith and Gent*, 2002] of Los Alamos National Laboratory (LANL). It resolves a free surface (i.e., no rigid lid) allowing for the use of high-resolution bathymetry and the determination of actual sea surface height and gradients. The dynamic-thermodynamic sea ice model is based on the work of *Hibler* [1979] with modifications by *Zhang and Hibler* [1997]. The model was initialized with three-dimensional temperature and salinity fields from the Polar Science Center Hydrographic Climatology (PHC) [*Steele et al.*, 2000] and integrated for 48 years in a spin-up mode. The 48-year spin-up consisted of 27 years of daily forcing using the 15-year mean annual cycle from ECMWF Climatology (1979–1993) followed by 6 repetitions of the 1979 daily annual cycle and then

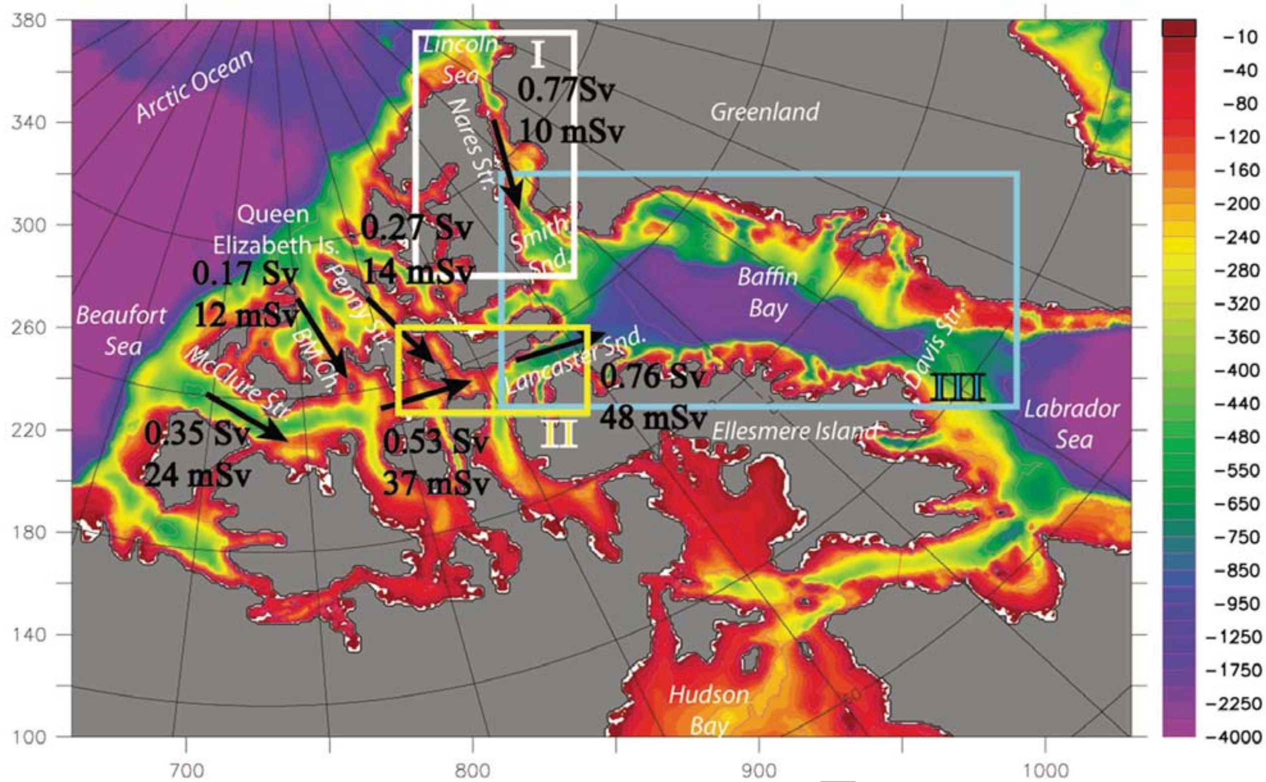

Figure 1. CAA bathymetry (m). Box I, Nares Strait region; box II, Lancaster Sound Region; box III, Baffin Bay region. The 26-year mean volume and freshwater fluxes are given in Sv and mSv respectively.

five repetitions of the 3-year period 1979–1981. The run used for our analyses was forced with daily averaged ECMWF data from 1979 to 2004. Additional details of the sea ice model, input of river runoff, and surface restoring have been provided elsewhere [*Maslowski and Lipscomb*, 2003; *Maslowski et al.*, 2004, 2007].

3. Nares Strait

[10] Nares Strait is located in the northeast corner of the CAA, providing a connection from the Lincoln Sea in the north to Baffin Bay in the south (Figures 1 and 2). It is bordered by Ellesmere Island to the west and Greenland to its east. Nares Strait is over 500 km long and its width ranges from ~35 km in the narrow channels to ~130 km in Kane Basin. Its depth varies from 600 m to ~220 m at the sill in Kane Basin. Nares Strait is a major outflow path for water exiting the Arctic Ocean.

[11] The modeled volume flux is almost entirely one way with net flow directed out of the Arctic Ocean. The model's strongest southbound flow, as shown by the distribution of velocity and TKE in Figure 2, is confined to a strong subsurface jet on the western side of the strait. There is some recirculation in Kane Basin and occasionally very weak northward flow along the eastern side of the strait. All of these features are in agreement with the observations [*Munchow et al.*, 2006, 2007; *Munchow and Melling*, 2008].

[12] The modeled 26-year mean net volume flux through Kennedy Channel (Figure 3a) is 0.77 Sv ± 0.17 Sv with considerable seasonal and interannual variation (0.4 Sv to 1.2 Sv). The modeled net liquid freshwater flux through Kennedy Channel (Figure 3b) has a 26-year mean value of 10.38 mSv ± 1.67 mSv. The 26-year freshwater flux time series shows an increase toward the end of the record which is not reflected in the volume flux time series but rather is due to decreasing upstream salinity, possibly associated with the modeled accelerated melt of multiyear ice to the north. The ice component is very small (Table 1), in part due to restrictions imposed by topography and the development of ice arches.

[13] The annual cycle of volume flux (Figure 4a) peaks in April and has a minimum in October. This is somewhat surprising as the maximum occurs when the strait has its thickest ice. However, *Munchow and Melling* [2008] observed the along channel vertically averaged flow near Ellesmere Island (which dominates the overall volume flux) to have a southward pulse from January to June and then diminish the rest of the year. This agrees with our model results. The origin of this pulse of volume flux will be further discussed in section 9. The annual freshwater flux cycle (Figure 4a) differs from the volume flux cycle as it has two peaks: one associated with the volume peak in March and a larger one in August due to seasonal ice melt and subsequent decrease of salinity.

[14] Observations from this location are rare but some contemporary data do allow for limited comparisons (Table 2). Model data show good agreement with the single month volume and freshwater flux estimates from *Munchow et al.* [2006] and with the multiyear volume flux data set (measured below 30 m depth due to hazards of sea ice) of

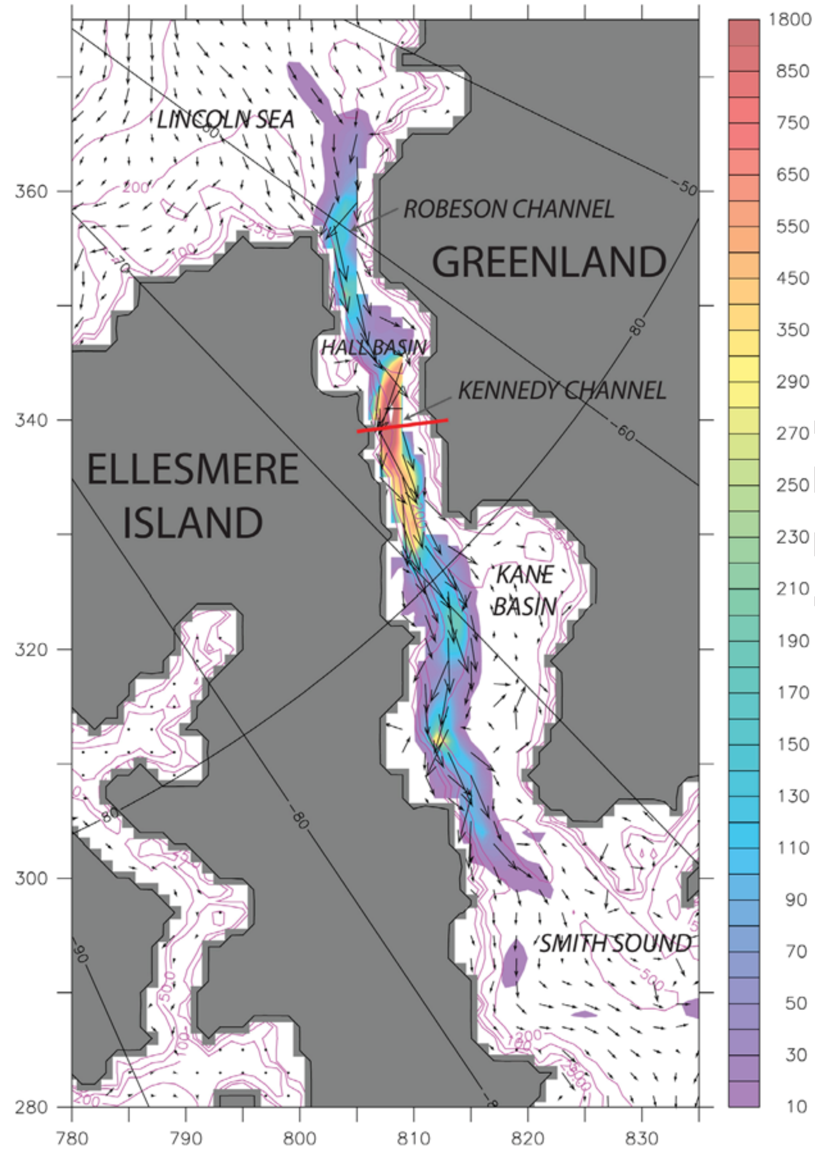

Figure 2. Nares Strait 0–122 m 26-year mean velocity (vectors) and TKE (shading). Red line is location of Kennedy Channel flux measurement.

Munchow and Melling [2008]. Modeled ice flux was an order of magnitude too low when compared with the estimates of *Kwok* [2005]. This discrepancy is most likely due to a combination of model resolution, ice arching (discussed further in the next section) and the lack of high resolution wind-forcing, specifically the effect of topographic funneling. *Samelson and Barbour* [2008] and *Samelson et al.* [2006] describe intense wind events and show evidence for atmospheric control of ice motion through Nares Strait.

[15] *Munchow and Melling* [2008] described an increasing trend in volume flux between 2003 and 2006. The model results also show an increasing trend in volume flux at these depths at the end of the record (where there is some overlap with the observations). The benefit of the model is that this trend can be put into context within a 26-year period. The modeled increase appears to be the flow simply recovering from of a period of anomalously low volume flux from 1998 to 2002, still well below previous maxima of 1990 and 1995 and inside the range of variability for the time series (Figure 3a).

[16] Usually the ice in Nares Strait is observed to consolidate between December and March in Smith Sound, forming an ice arch which prevents the export of thick multiyear ice from the Arctic to Baffin Bay [*Dunbar*, 1973; *Barber et al.*, 2001; *Kwok*, 2005]. Another ice arch typically develops above Robeson Channel at the northern extent of Nares Strait [*Kwok et al.*, 2010]. Our model reproduces the ice arches above Robeson Channel, in Smith Sound, and one in Kennedy Channel. However, these ice arches are most likely overrepresented, as model ice strength is based upon the mean thickness of the ice, rather than the thinner ice which experiences more deformation [*Maslowski and Lipscomb*, 2003]. The modeled ice arch above Robeson Channel is perennial; it moves slightly north and south throughout the time period but it is always there. This could be partially due to excessive ice strength and insufficient model resolution in

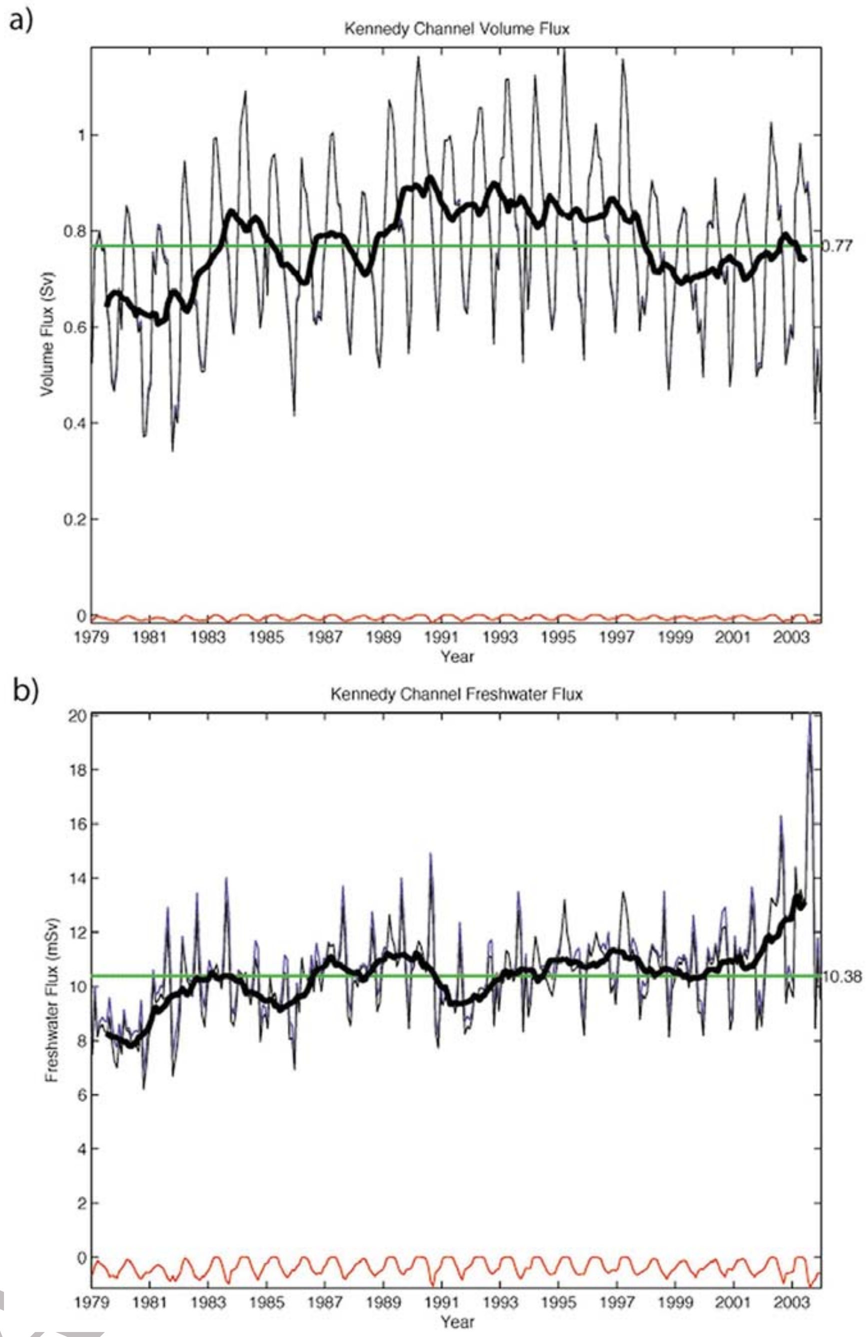

Figure 3. Model 26-year fluxes through Kennedy Channel (blue, southward; red, northward; black, net; thick black, 13-month running mean of the net): (a) volume and (b) freshwater (liquid).

the channel which could explain why our modeled ice flux is consistently lower than in reality. As far as model ice goes there is no connection with the Arctic Ocean via Nares Strait, and the small amount of sea ice exported through the southern end in Smith Sound has been created within the strait. The modeled ice arch in Smith Sound is more variable; in several years the North Water Polynya expands northward across the arching location. The final simulated ice arch appears in the narrow Kennedy Channel where ice is confined, resulting in higher ice concentration and thickness which prevents further southward motion. This has been

Table 1. Model 26-Year Mean (Monthly Standard Deviation) Volume and Freshwater Fluxes (Liquid and Solid)

Location	Volume Flux (Sv)	FW Flux (mSv)	FW Flux Ice (mSv)
Nares Strait	0.77 (0.17)	10.38 (1.67)	0.80 (0.75)
Lancaster Sound	0.76 (0.12)	48.45 (7.83)	1.24 (1.55)
Davis Strait	1.55 (0.29)	62.66 (11.67)	12.81 (13.09)
Fram Strait	2.33 (0.57)	12.17 (5.24)	51.54 (37.41)

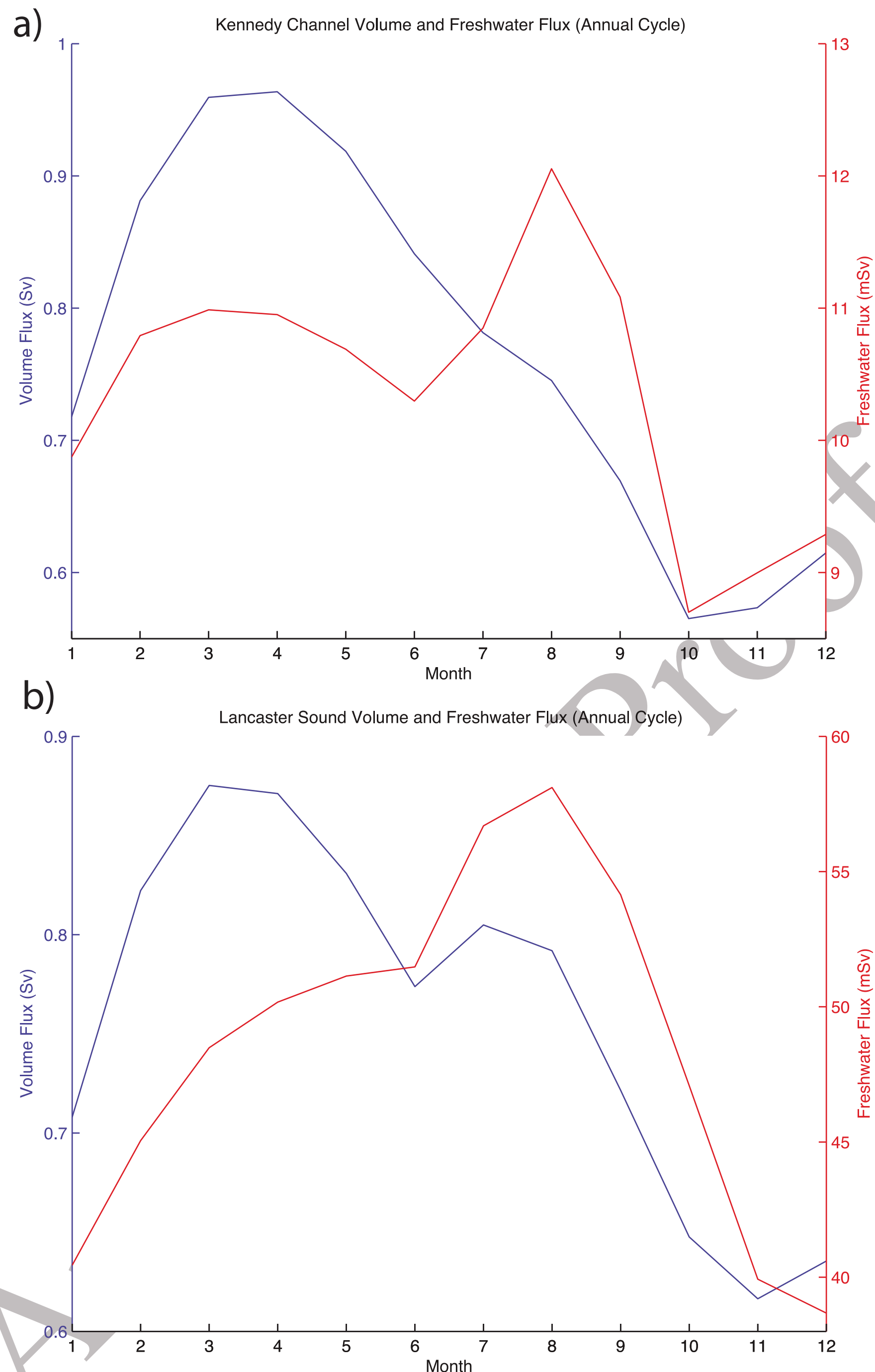

Figure 4. Net flux annual cycles (blue, volume; red, freshwater (liquid)) through (a) Kennedy Channel and (b) Lancaster Sound.

observed [*Kwok et al.*, 2010] but does not appear to last as long as it does in the model.

4. Lancaster Sound

[17] Lancaster Sound is the other location for major CAA outflow (Figure 5). It opens to northwestern Baffin Bay and is due north of Baffin Island. Its opening is about 100 km wide and it is 700–800 m deep at its mouth. Flow though Lancaster Sound comes from the west, as a combination of the inputs from several gateways from the Arctic Ocean to the CAA (Figure 1). Moving from west to east, flow originates in McClure Strait, gets an addition from Byam Martin Channel in the north, continues eastward flowing through Barrow Strait, receives more input from Penny Strait to the north, and then proceeds through Lancaster Sound to Baffin Bay. Deep flow is restricted by the presence of shallow sills located in the vicinity of Byam Martin Channel, Barrow Strait, and Penny Strait. Mean individual volume and freshwater fluxes for several straits in the CAA are shown in Figure 1.

Table 2. Comparisons Between NAME Model Mean (Standard Deviation) Fluxes and Available Observations

Study	Type	Location	Period	Volume Flux (Sv)	FW Flux (mSv)	FW Flux Ice (mSv)
Munchow et al. [2006]	observation	Nares Strait	Aug 2003	0.8 (0.3)	25 (12)	–
NAME	model	Nares Strait	Aug 2003	0.83	18.97	–
Munchow and Melling [2008]	observation	Nares Strait (30 m to bottom)	Aug 2003 to Aug 2006	0.57 (0.09)	–	–
NAME	model	Nares Strait (30 m to bottom)	Aug 2003 to Aug 2004	0.54 (0.11)	–	–
NAME	model	Nares Strait (30 m to bottom)	1979–2004	0.61 (0.13)	–	–
Kwok [2005]	observation	Nares Strait	1996–2002	–	–	4
NAME	model	Nares Strait	1996–2002	–	–	0.11 (0.30)
Prinsenberg and Hamilton [2005]	observation	western Lancaster Sound	1998–2001	0.75 (0.25) annual SD	46.3	–
NAME	model	western Lancaster Sound	1998–2001	0.72 (0.04) annual SD	44.31	–
Melling et al. [2008]	observation	western Lancaster Sound	Aug 1998 to Aug 2004	0.7 – range (0.4–1.0)	48	–
NAME	model	western Lancaster Sound	Aug 1998 to Aug 2004	0.74 – range (0.69–0.78)	47.18	–
Cuny et al. [2005]	observation	Davis Strait	Sep 1987 to Sep 1990	2.6 (1.0)	92 (34)	16.7
NAME	model	Davis Strait	Sep 1987 to Sep 1990	1.7 (0.3)	66 (14)	14.8
Schauer et al. [2004]	observation	Fram Strait	Sep 1997 to Aug 2000	between 2(2) and 4(2)	–	–
NAME	model	Fram Strait	1979–2004	2.33 (0.57)	–	–
De Steur et al. [2009]	observation	Fram Strait	1998–2008	–	66 (25.7)	–
Kwok et al. [2004]	observation	Fram Strait	1991–1998			70
NAME	model	Fram Strait	1979–2004	–	12.2 (5.2)	51.5 (37.4)
Straneo and Saucier [2008]	observation	Hudson Strait (outflow only)	–	–	78–88	–
NAME	model	Hudson Strait (outflow only)	–	–	15.31	–
Dickson et al. [2007]	observation	Hudson Strait	–	–	42	–
NAME	model	Hudson Strait	–	–	9.59	–

[18] The modeled net volume flux through the mouth of Lancaster Sound is into Baffin Bay, but there is a deep inflow on its northern side that extends to the surface in summer (Figure 5b). In the model, this flow recirculates and heads back out toward Baffin Bay well before it reaches Prince Regent Inlet, in agreement with summertime drifter and mooring observations [*Fissel et al.*, 1982].

[19] At the mouth of Lancaster Sound where the flow enters Baffin Bay, the model 26- year mean net volume (Figure 6a) and liquid freshwater fluxes (Figure 6b) were 0.76 Sv $\pm$ 0.12 Sv and 48.45 mSv $\pm$ 7.83 mSv respectively. Ice fluxes accounted for an additional freshwater liquid equivalent of 1.24 mSv $\pm$ 1.55 mSv, bringing the combined freshwater flux to 49.69 mSv $\pm$ 8.61 mSv. Liquid freshwater fluxes are mostly a function of the volume fluxes, which is reflected in the model correlation between the volume and freshwater flux time series (R = 0.85 at 0 lag), similar to the model study of *Jahn et al.* [2010]. It is important to note that although Lancaster Sound accounts for slightly less volume flux (26-year mean) than Nares Strait, it accounts for almost 5 times its long-term mean freshwater flux. This is probably due to a combination of more direct linkage to low salinity Pacific water, large freshwater input of the Mackenzie River, and seasonal input of water derived from the melting of ice in the Beaufort Sea. The magnitude and multiple sources of freshwater flux through the Northwest Passage might be the reason why the ice-melt contribution at the end of the record is less pronounced than in Nares Strait.

[20] The annual net volume flux cycle has dual maxima, the larger one in March and the secondary maximum in July (Figure 4b). The minimum flux is in November with a secondary minimum in June. Like in Nares Strait, the overall maximum volume flux occurs when the strait has its thickest ice cover. The origin of both pulses in volume flux will be further discussed in section 9. Unlike in Nares Strait, the annual freshwater flux cycle has only one peak at the end of summer, not one associated with the overall volume maximum (Figure 4b). This is in part due to a loss of about 4.5 mSv of freshwater southwards through Prince Regent Inlet in February/March (not shown). This reduces the winter peak in the freshwater annual cycle, which is visible in the model throughout the CAA as far as the western Lancaster Sound mooring array (Figure 5). Without this loss, the freshwater cycle would possibly have two peaks.

[21] Observational data is relatively most abundant in the western Lancaster Sound and Barrow Strait region (Figure 5). As such, model fluxes were calculated for the western Lancaster Sound mooring array section to allow for comparisons (Table 2). Model volume and freshwater fluxes showed good agreement with contemporary 3- and 6-year data sets [*Prinsenberg and Hamilton*, 2005; *Melling et al.*, 2008]. However, it should be noted that the observed standard deviation (annual) was much larger. In general, the smaller modeled standard deviations could be due to the large scale smoothed atmospheric forcing, which misses small scale (spatial and temporal) variation. Gustiness of winds, funneling due to topography, and intense drainage (katabatic) phenomena are not represented in the model. However, they may have significant effects on the observations, especially since the observations are based on few points. As with the model data, freshwater flux appears to be almost entirely a function of volume flux [*Melling et al.*, 2008; *Prinsenberg et al.*, 2009].

[22] It is generally accepted that volume flux through Barrow Strait/western Lancaster Sound peaks in late summer. After geostrophic calculations from an August 1998 hydrographic section showed an eastward current extending 2/3 of the distance across the sound with the highest speed near the southern shore, it was concluded that the flow peaks in August on the southern side of the strait [*Melling et al.*, 2008]. Flow on the northern side of the strait was shown to be quite variable and contributed little to the net flux on a long-term average [*Prinsenberg and Hamilton*, 2005;

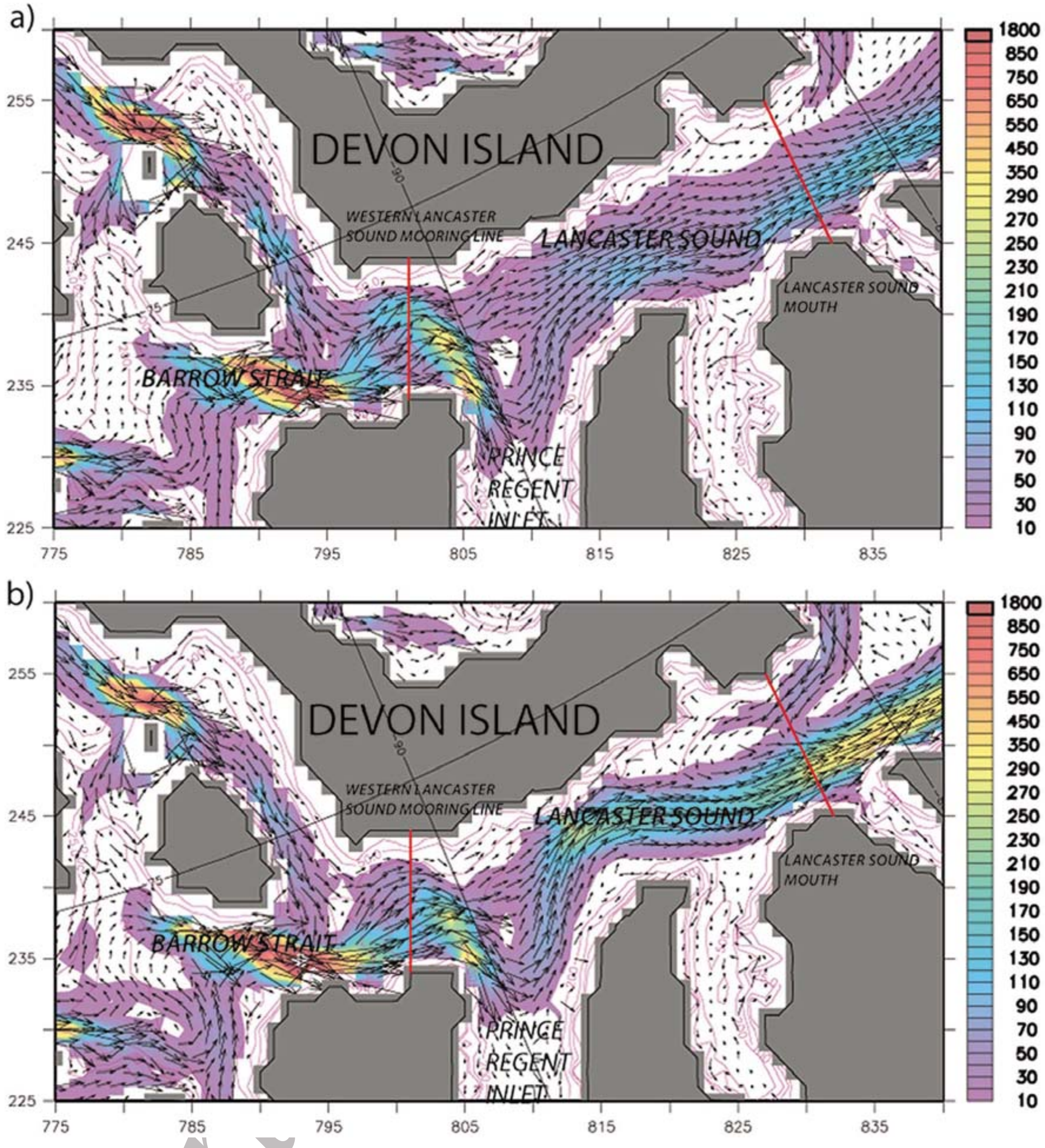

Figure 5. Lancaster Sound 0–122 m 26-year mean velocity (vectors) and TKE (shading): (a) March and (b) August.

Melling et al., 2008; *Prinsenberg et al.*, 2009]. As a result, estimated fluxes for the entire section were based on weighted observations from the southern moorings [*Prinsenberg and Hamilton*, 2005].

[23] To investigate the flow on either side of the strait, modeled annual volume flux cycles were calculated for the entire western Lancaster Sound section and separately for the north and south sections of the line (Figure 7). The modeled flow on the southern side of the channel peaks in August (also see Figure 5b) in agreement with the observations [*Prinsenberg and Hamilton*, 2005; *Melling et al.*, 2008; *Prinsenberg et al.*, 2009]. However, model flow on the northern side of the channel has an annual peak in March, which is also evident in the distribution of depth-averaged velocity and TKE in Figure 5a. This is particularly evident in long-term monthly mean model cross sections, where the core of the flow is observed to change sides of the channel (Figure 8). At the time of the August 1998 hydrographic section, flow along the northern side of the channel was decreasing toward the minimum of its annual cycle (Figures 7 and 8), which possibly lead to the determination of flow there as being variable and contributing little to the net flux.

[24] Using 2001–2004 mooring data only for the southern half of the transect, *Melling et al.* [2008] present velocity peaks only in August/September (see their Figure 9.5). This is in agreement with model results when considering the same area (i.e., only the southern portion). Furthermore,

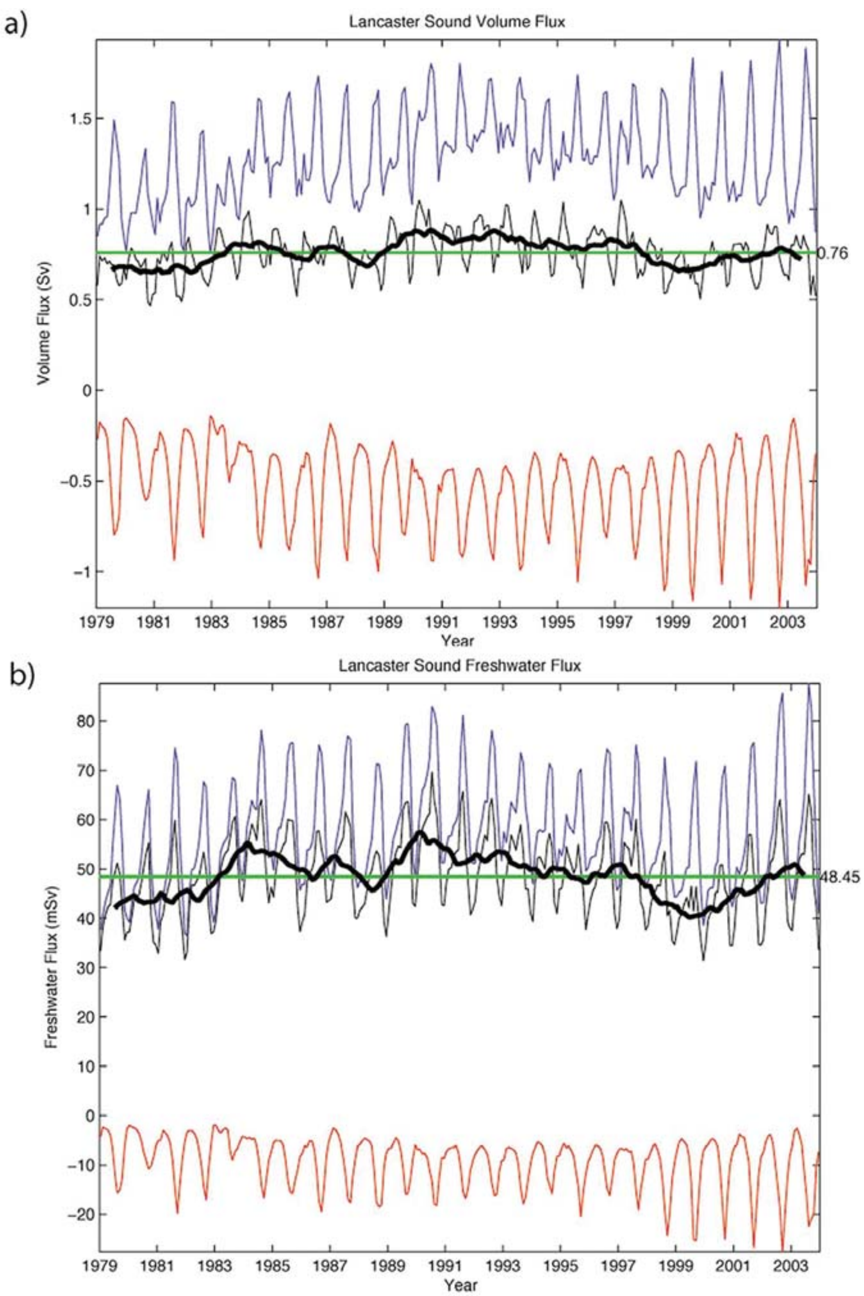

Figure 6. Lancaster Sound fluxes (blue, southward; red, northward; black, net; thick black, 13-month running mean of the net): (a) volume and (b) freshwater (liquid).

under closer investigation of their plot one can make an argument that as one moves across the mooring array toward the northern side that the volume flux regime changes from one with a summertime peak to one with a wintertime peak. Additionally, observed volume fluxes in western Lancaster Sound [*Prinsenberg and Hamilton*, 2005] reveal not only a late summer maximum but also some evidence of a relative maximum in winter (∼March). Using data from the same moorings, *Peterson et al.* [2008] briefly mention that there is some evidence of a secondary maximum in the transport annual cycle in February (see their Figures 2a and 3a) and there also appears to be a February/March relative maximum in the mooring data as presented by *Melling et al.* [2008] (see their Figure 9.7). *Prinsenberg et al.* [2009] noted that the northern flow is generally directed toward the west in summertime and to the east in wintertime. These observations of wintertime eastward flow are in agreement with our model results. The observed negative (westward) flow along the northern edge in summer has been attributed to a coastal buoyancy current. This feature may require higher resolution to simulate, beyond the capabilities of our 9 km model.

[25] Given that the structure of the modeled flow in western Lancaster Sound differs significantly from the scaled up observations, it is difficult to explain the agreement in volume and freshwater flux values. Additional details on how the observations of the southern end of the

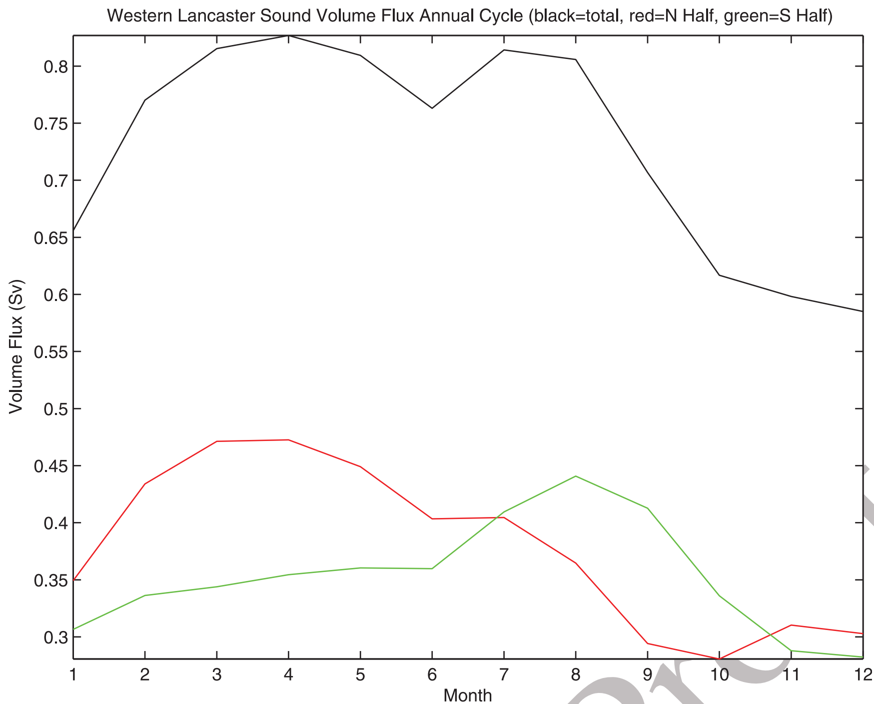

Figure 7. Model annual cycle (based on August 1998–2004) of volume transport across western Lancaster Sound line of moorings (black, total section; red, northern half of section; green, southern half of the section).

strait were scaled to represent the total section would be necessary for a more detailed comparison.

5. CAA Sea Ice

[26] CAA sea ice cover undergoes a large annual cycle (Figure 9). The CAA forms and melts sea ice locally. Wintertime ice concentration routinely reaches near 100% but the summertime minimum area decreases, especially toward the end of the study period. Likewise, ice volume decreases with accelerated loss toward the end of the record. Modeled thick multiyear ice is confined to the north due to ice arching above Penny Strait and Byam-Martin Channel and cannot enter the Northwest Passage from that direction. However, the model shows a tongue of thick ice entering via McClure Strait in the west, blocking that end of the Northwest Passage. Satellite based ice flux estimates from recent years [*Kwok*, 2006, 2007; *Agnew et al.*, 2008] have shown the CAA to not only create but also export sea ice via Lancaster Sound, Amundsen Gulf, and McClure Strait. In the model, ice is exported through Lancaster Sound, Amundsen Gulf imports and exports ice, but McClure Strait imports a small amount. The discrepancies are likely due to modeled ice being less mobile than has been observed. *Lietaer et al.* [2008] used a finite element numerical model that yielded CAA ice export to Baffin Bay 1979–2005 annual mean of 125 km^3 yr^{-1}. Our model results accounted for just over 1/3 of that value, again suggesting that ice mobility could be an issue.

6. Davis Strait

[27] Davis Strait lies between southern Baffin Island and Greenland. It divides Baffin Bay in the north from the Labrador Sea to the south. There is a ~670 m deep sill that constricts the flow in the vertical as well as the horizontal narrowing of the strait and preventing deep flow from Baffin Bay to the Labrador Sea. On the western side of Davis Strait, the Baffin Island Current (BIC) carries cold and fresh water of mostly Arctic origin to the south, while on the eastern side of the strait the West Greenland Current (WGC) flows northward carrying warmer and saltier Irminger Water.

[28] After the CAA outflow moves into Baffin Bay, it is exported southwards to the Labrador Sea via Davis Strait. The modeled 26-year mean net volume (Figure 10a) and liquid freshwater fluxes (Figure 10b) through Davis Strait (positive values are southward into the Labrador Sea) are 1.55 Sv $\pm$ 0.29 Sv and 62.66 mSv $\pm$ 11.67 mSv respectively. Ice flux accounts for an additional liquid equivalent flux of 12.81 mSv $\pm$ 13.09 mSv giving a total mean freshwater flux of 75.48 $\pm$ 9.73 mSv. The model volume, freshwater and ice fluxes for September 1987–1990 were within the bounds of the estimates determined by *Cuny et al.* [2005] (Table 2). *Curry et al.* [2011] obtained similar results for September 2004–2005.

[29] Model volume and liquid freshwater flux anomalies correlated with R = 0.75, less than the correlation at Lancaster Sound (R = 0.85), suggesting modification of the signal within Baffin Bay. Recalculating the correlation using the combined freshwater flux anomaly (including the ice component instead of just the liquid freshwater) yields a value of R = 0.81, capturing an additional 10% of the variance. Thus our combined freshwater and volume flux anomalies are highly correlated at Davis Strait. This fact reflects the dominance of freshwater flux contribution from Lancaster Sound and much less from Nares Strait, where freshwater and volume fluxes were not significantly correlated.

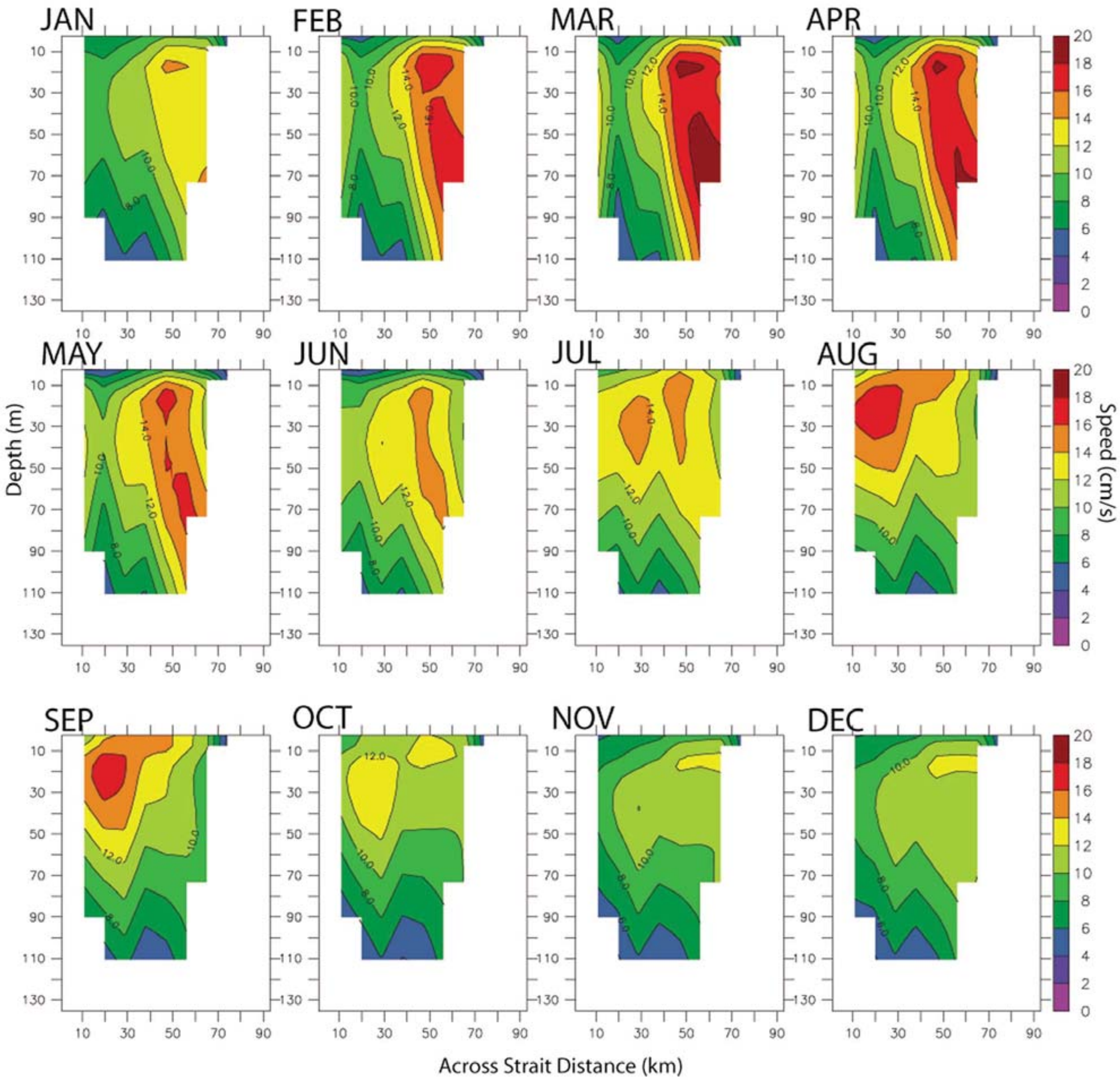

Figure 8. Monthly cross sections of flow (cm/s) through western Lancaster Sound. Southern side of the section is on the left and northern end is on the right. Positive values indicate flow moving towards the east.

[30] The annual cycle of volume flux (Figure 11a) shows that the net peak outflow southwards through Davis Strait occurs in the winter months (February/March/April), when both northward and southward fluxes are at their minimum (the northward flux happens to reduce much more than the southbound flux, leaving the net at its maximum) (Figure 11a). This is similar to *Cuny et al.* [2005] who observed that the northward volume flux was at a minimum in March/April and the minimum southward flux was in March. The most vigorous fluxes across the strait occur when the area is ice free in September but largely cancel one another in the net sense. *Cuny et al.* [2005] also observed from 1987 to 1990 that the highest northward and southward fluxes (volume and freshwater) to occur concurrently, but in November. *Tang et al.* [2004] observed the strongest northward flux in eastern Davis Strait to occur in fall as well. The annual cycle of freshwater flux peaks at the end of the melt season in September (Figure 11b).

7. Fram Strait

[31] The other pathway for freshwater to exit the Arctic Ocean is via Fram Strait. Fram Strait lies with Greenland to its west and Svalbard to its east. It is a both an entry and exit point for volume fluxes of the Arctic Ocean. On its eastern side the West Spitsbergen Current (WSC) flows northward along Svalbard into the Arctic Ocean and to the west the East Greenland Current (EGC) flows southwards out of the Arctic Ocean.

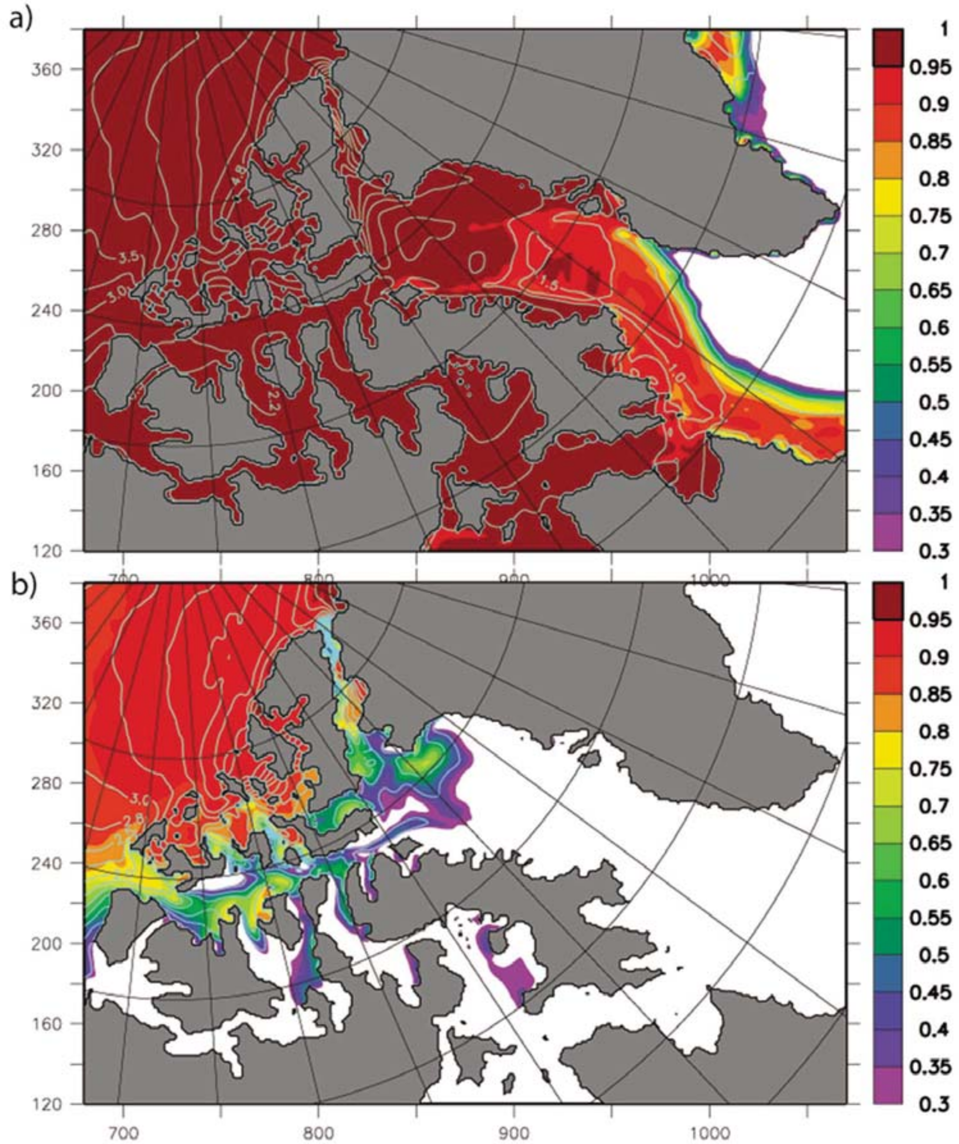

Figure 9. The 26-year model mean ice concentration (shading) and thickness (contours): (a) March and (b) September.

[32] In the net volumetric sense Fram Strait is an export pathway. The model 26-year mean volume flux (from the Arctic Ocean to the south) through Fram Strait is 2.33 Sv ± 0.57 Sv. This is within the bounds of the observational estimates of *Schauer et al.* [2004] (Table 2). The model northward and southward volume fluxes are 6.4 Sv and 8.73 Sv respectively [*Maslowski et al.*, 2004]. They are smaller than estimates for 1997–2000 by *Schauer et al.* [2004], which are 9–10 Sv and 12–13 Sv respectively. However, the updated estimate of long-term (1997–2010) volume transport in the WSC across the same mooring array is 6.6 Sv ± 0.4 Sv (A. Beszczynska-Möller et al., Variability of Atlantic water properties and transport in the entrance to the Arctic Ocean in 1997–2010, submitted to *ICES Journal of Marine Science*, 2011). The model 26-year mean freshwater (liquid) flux of 12.17 mSv ± 5.24 mSv is much lower than the flux of 66 mSv reported by *de Steur et al.* [2009], whose estimate combined limited in vertical measurements of the East Greenland Current (6 moorings with two shallowest instruments at depths below 50 m and below 200 m over ~150 km distance between 0° and 6.5°W) and 28-km and 33-level model results on the shelf (Table 2). However, most of the freshwater comes out as ice which accounts for an additional flux of 51.54 mSv ± 37.41 mSv, making the combined freshwater export to be 63.72 ± 39.18 mSv. This is in reasonable agreement with *Kwok et al.* [2004], who using ice aerial flux and limited thickness data estimated the ice outflow to be equivalent to ~70 mSv. To summarize (in the 26-year mean sense), Fram Strait exports about 1.5 times more net volume from the Arctic than does the CAA through Davis Strait. However, the CAA exports about 20% more FW than Fram Strait. It is important to note the large variability of the Fram Strait freshwater fluxes. Most of this variability is due to the ice component, which is largely wind controlled [*Kwok et al.*, 2004].

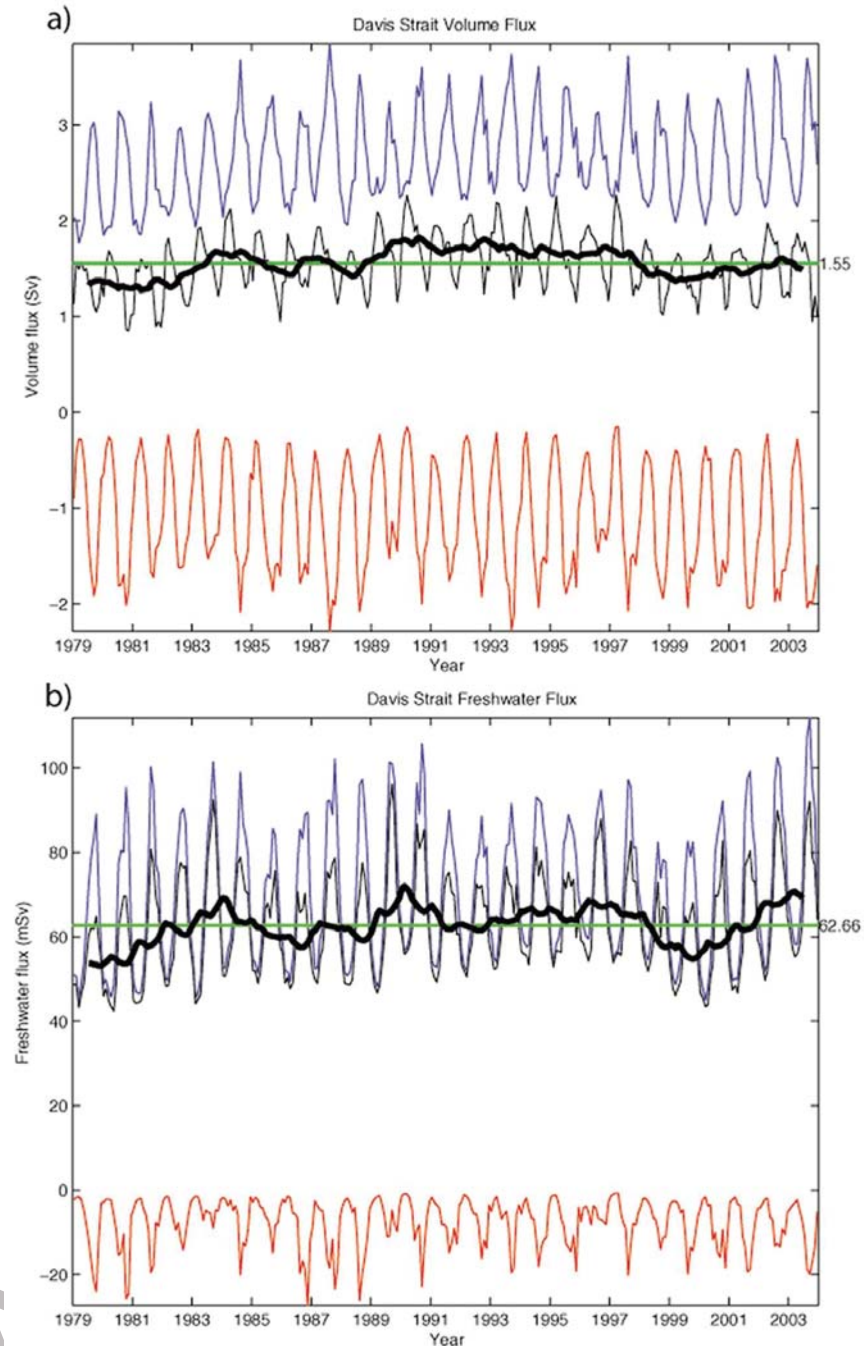

Figure 10. Davis Strait fluxes (blue, southward; red, northward; black, net; thick black, 13-month running mean of net): (a) volume and (b) freshwater (liquid).

[33] The model annual cycle of Fram Strait's net volume flux is at a minimum in April/May and has its maximum in November. It is nearly out of phase with the net volume flux through Nares Strait (maximum in April and minimum in October). Given the uncertainties in observational estimates of directional fluxes through Fram Strait (due to high current variability, recirculation and spatial coverage [*de Steur et al.*, 2009; Beszczynska-Möller et al., submitted manuscript, 2011]), direct comparison of the annual cycle of net volume flux is not readily obtainable.

[34] A large part of the freshwater exported via Fram Strait is lost due to the eastward recirculation from EGC in the southern Greenland Sea. A shortcoming of the model is that it advects ice too far to the east in the Iceland Sea, effectively removing some freshwater from the southward flow of EGC. However, the remaining freshwater is continually mixed and diffused (especially with the northward flowing warm and salty Irminger Current) as it is carried south toward Denmark Strait. There, the relative amount of freshwater flux continues to shift phase from being predominantly ice to liquid. Further to the south, mixing

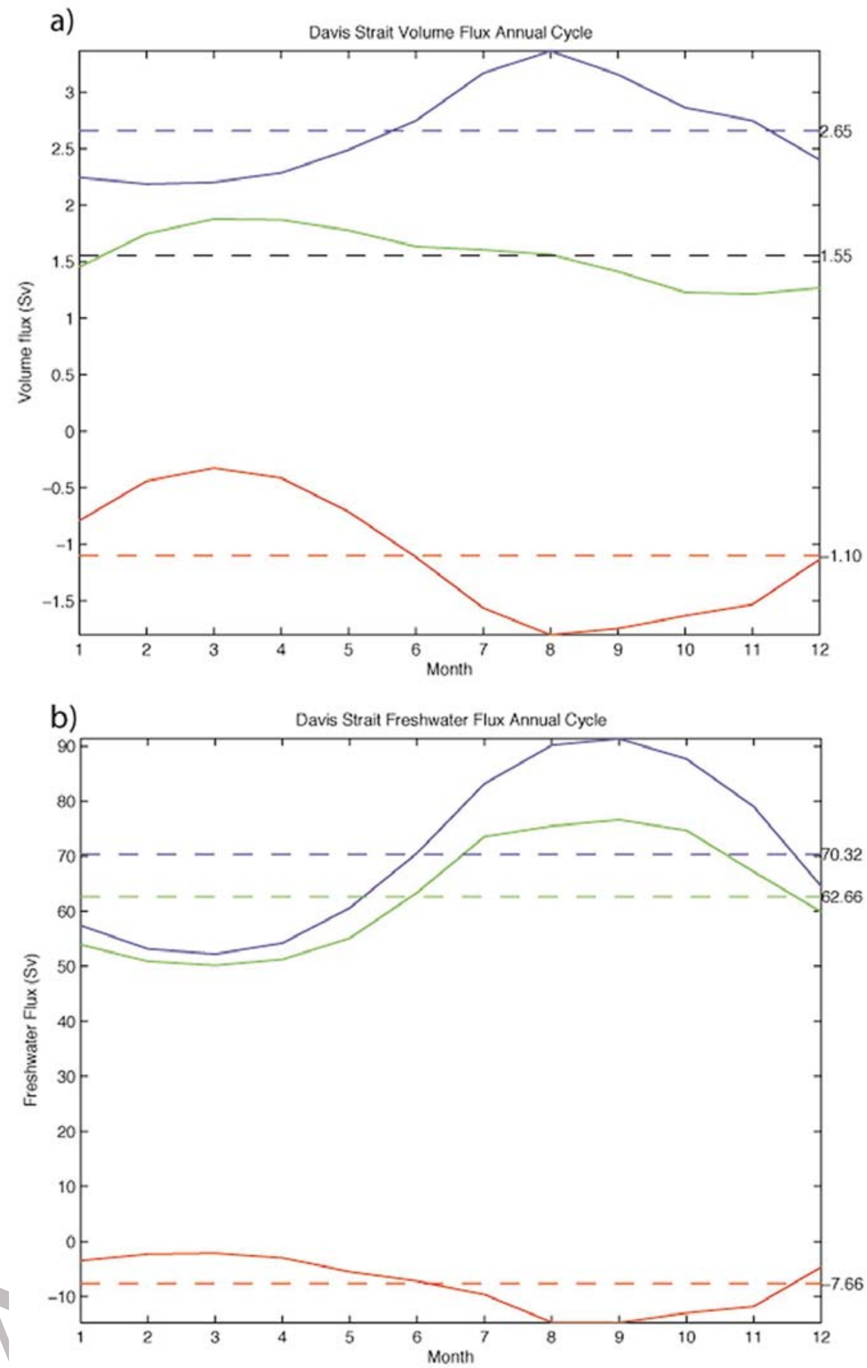

Figure 11. Davis Strait flux annual cycles: (a) volume (blue, southward; red, northward; black, net) and (b) net freshwater (liquid) (blue, southward; red, northward; black, net).

continues in the Irminger Sea except in the East Greenland Coastal Current (EGCC), which is likely not resolved at the 9-km grid and is missing freshwater run from Greenland [*Sutherland and Pickart*, 2008]. Some of the remaining flow retroflects to the east at Cape Farewell so very little of the original freshwater exported from Fram Strait makes it to the Labrador side of Greenland (1.70 mSv ± 2.07 mSv compared to the 63.72 mSv ± 42.65 mSv that transited Fram Strait), contributing to a local high salinity bias in the model [*McGeehan and Maslowski*, 2011]. The remaining freshwater then either splits into a branch moving westward as it traverses the northern rim of the Labrador Sea or it continues to the north through Davis Strait. Based on this model results referenced to salinity of 34.8, the Fram Strait branch provides very little freshwater to the vicinity of the Labrador Sea compared with the CAA pathways that deliver 75.48 mSv ± 24.76 mSv via Davis Strait.

8. Hudson Bay

[35] Hudson Bay is another freshwater source to the Labrador Sea. While not usually regarded as a connection

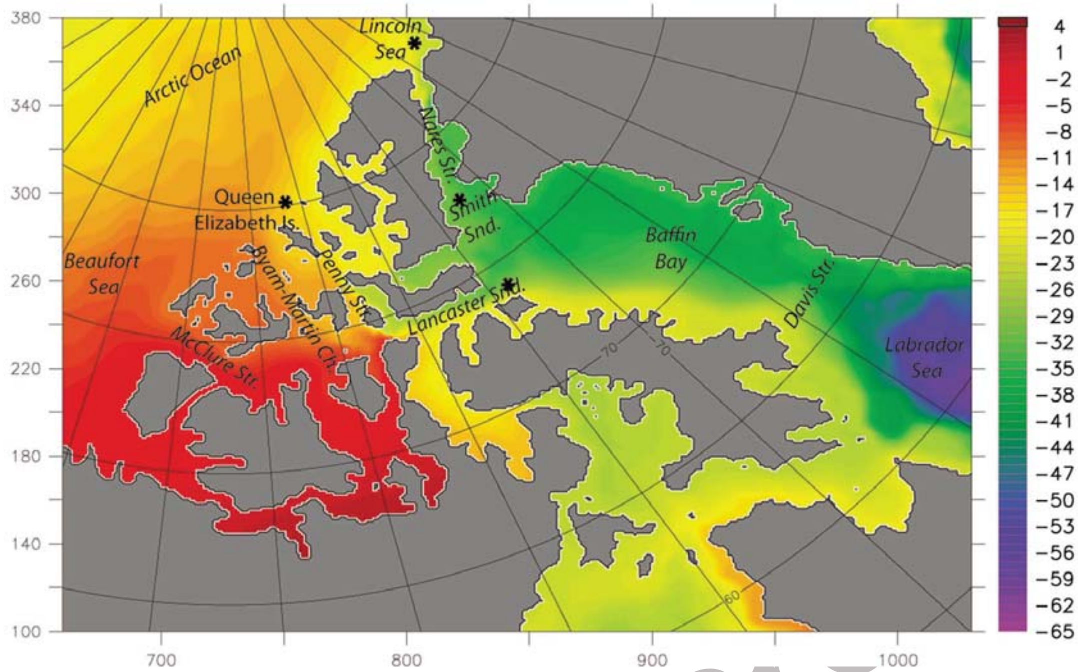

Figure 12. Model 26-year mean CAA SSH (cm). Asterisks denote endpoints of SSH gradients discussed in text. Heights are relative to the geoid.

between the Arctic Ocean and the Labrador Sea or even a passageway of the CAA, it does connect to the CAA (via the very narrow Fury and Hecla Strait) and it opens onto the Labrador shelf.

[36] The Hudson Strait 26-year mean net volume flux is nearly balanced, accounting for just 0.17 Sv of net flow toward the Labrador Sea. However, the net liquid freshwater flux is 9.58 mSv and the ice flux is 0.67 mSv, bringing the combined freshwater flux to 10.25 mSv. This is drastically lower than the 42 mSv net freshwater estimate of and the outflow only values are less than 20% of those observed [*Straneo and Saucier*, 2008] (Table 2). This disagreement is likely due to the fact that the model has no explicit river input to Hudson Bay (that accounts for more than 80% of the total freshwater flux [*Dickson et al.*, 2007]), except the surface salinity restoring, which does not appear to be sufficient to make up for the entire riverine source. Also at 9 km resolution the model lacks complete depiction of flows in Hudson Bay and Hudson Strait, particularly their coastal currents. In any event, Hudson Bay provides a significant input to the Labrador shelf, especially in comparison to the Fram Strait branch.

9. Control Mechanisms

9.1. Previously Proposed Control Mechanisms

[37] The observed freshwater flux through the CAA is largely a function of volume flux [*Melling et al.*, 2008; *Prinsenberg et al.*, 2009]. As such, it is imperative to identify controls on the volume flux in order to understand freshwater flux. Volume flux through the CAA is generally believed to be due to a background sea surface height (SSH) gradient between the northern Pacific Ocean, Arctic Ocean, and northern Atlantic Ocean. It is due in large part to steric height, i.e., fresher less dense water in the North Pacific that increases in salinity (causing increased density and decreased SSH) as it moves through the Arctic and into the North Atlantic [*Steele and Ermold*, 2007]. The annual cycle of volume flux through western Lancaster Sound has been attributed to a seasonal modulation of the SSH gradient [*Prinsenberg and Bennett*, 1987]. Recent analyses correlating Arctic winds and oceanic volume fluxes through western Lancaster Sound suggest that summer winds located along the CAA's Beaufort coast blowing toward the northeast cause an Ekman transport of mass toward the CAA. This in turn leads to increased setup and ultimately increased volume flux through the CAA, resulting in a summertime flux maximum [*Peterson et al.*, 2008; *Prinsenberg et al.*, 2009]. However, studies of the forcing behind the volume flux through the CAA passages are severely limited by a lack of SSH observational measurements across the CAA.

[38] This model provides contemporary SSH and flux information so the two can be investigated together. Additionally, it provides 26 years of monthly output, allowing for examination of seasonal cycles and interannual variability. The modeled 26-year mean SSH plot (Figure 12) shows a background SSH gradient across the CAA, in accordance with *Steele and Ermold* [2007]. This provides a background forcing for flow through the CAA. However, the processes controlling the annual cycle of volume flux are not fully understood.

9.2. Summer Volume Flux Maximum

[39] Model results for volume flux through Lancaster Sound reveal two peaks in the annual cycle: one in March and a smaller one in July (Figure 4b). The relative maximum occurring in the late summertime is consistent with observations. Furthermore, the peak does appear due to the wind. When only considering volume fluxes for the upper 25 m, both peaks in the annual cycle are still present but the larger

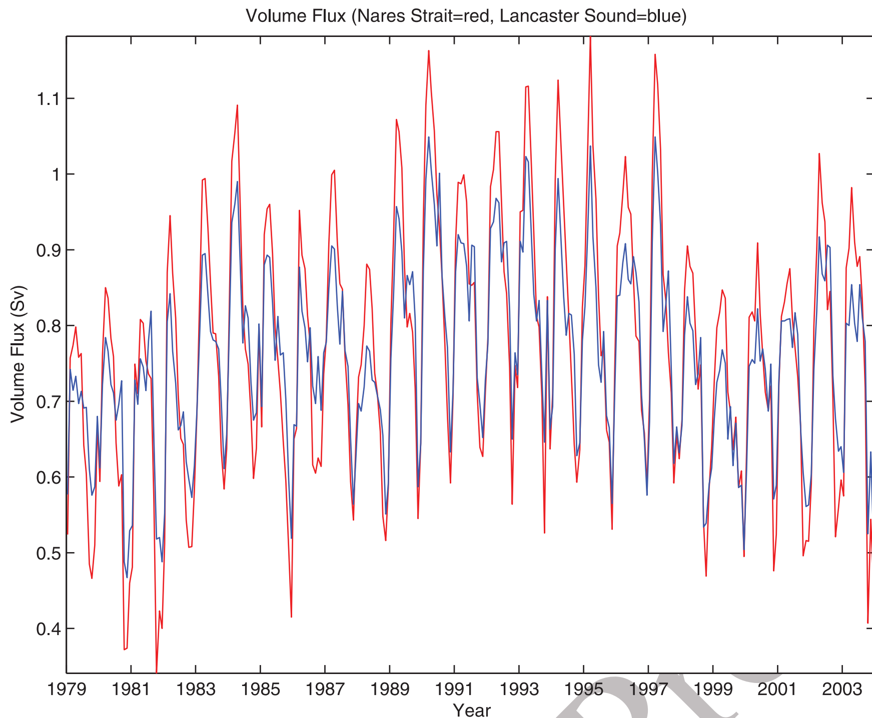

Figure 13. The 26-year net volume fluxes. Nares Strait (red) and Lancaster Sound (blue).

one occurs during the late summer instead of during the late winter (as it does when considering all depths). This occurs for the length of the CAA, with annual cycles of the upper 25 m volume flux at McClure Strait, Byam Martin Channel, and Penny Strait all behaving like Lancaster Sound with the larger peaks occurring in late summer. This is the time with the climatological wind most favorable to flow through the CAA (excluding Nares Strait) and the time when the ice has retreated, allowing wind to act more on the ocean surface. This also explains why there is not a late summer pulse of volume through Nares Strait. The wind direction is not conducive to increased summertime flow and Nares Strait has typically retained more of its ice cover than the Northwest Passage anyways, insulating the ocean from the overlying winds.

9.3. Winter Volume Flux Maximum

[40] The annual cycle of volume flux through Nares Strait has only one maximum, in March/April (Figure 4a). This coincides with the larger maximum volume flux through Lancaster Sound (Figure 4b). When considering fluxes integrated over all depths, this annual peak in modeled volume flux does not appear related to the wind-forcing. This is consistent with the findings of *Munchow and Melling* [2008] who determined that Nares Strait volume fluxes below 30 m were independent of the wind. Furthermore, when the time series of volume fluxes for both locations are plotted together (Figure 13), it becomes apparent that although the annual cycles are different (one or two volume peaks), most of the variability is common to both locations (correlation R = 0.94). This suggests a common large scale forcing. Although the upstream ends of both locations are different, they do share their downstream endpoint: i.e., northern Baffin Bay.

9.4. SSH Gradients

[41] Results from a modeling study by *Kliem and Greenberg* [2003] suggested that the volume flux through the CAA is a function of the Arctic to Baffin Bay SSH gradient, whereby the fluxes are modulated by a change in SSH in Baffin Bay. They calculated that decreasing the SSH in Baffin Bay by 5 cm would double the volume flux through the CAA. Unfortunately they only simulated summertime conditions in the CAA. *Houssais and Herbaut* [2011] conducted a more recent modeling study that also determined flow through Nares Strait responds to downstream SSH changes. Their work relied on annual means, leaving the question of annual cycles unaddressed.

[42] Our model results based on 26-years of simulation with monthly output demonstrate that SSH gradients (calculated between two points north and south of each passage, which are denoted with asterisks shown in Figure 12) do explain the annual peak volume fluxes (around March) through both Nares Strait (Figure 14a) and Lancaster Sound (Figure 14b). The volume flux anomalies and SSH gradient anomalies are also highly correlated. Volume flux anomalies through Nares Strait (Figure 15a) and anomalies of the SSH gradient (measured from the Lincoln Sea to Smith Sound) (Figure 15b) were highly correlated (R = 0.89). Volume flux anomalies through the mouth of Lancaster Sound (Figure 15c) and anomalies of the SSH gradient (measured between the Queen Elizabeth Islands and western Baffin Bay) (Figure 15d) were also highly correlated (correlation R = 0.85).

[43] For Nares Strait, about half of the variance in the SSH gradient anomalies corresponded to SSH anomalies upstream in the Lincoln Sea and the other half corresponded to negative SSH anomalies downstream in Smith Sound,

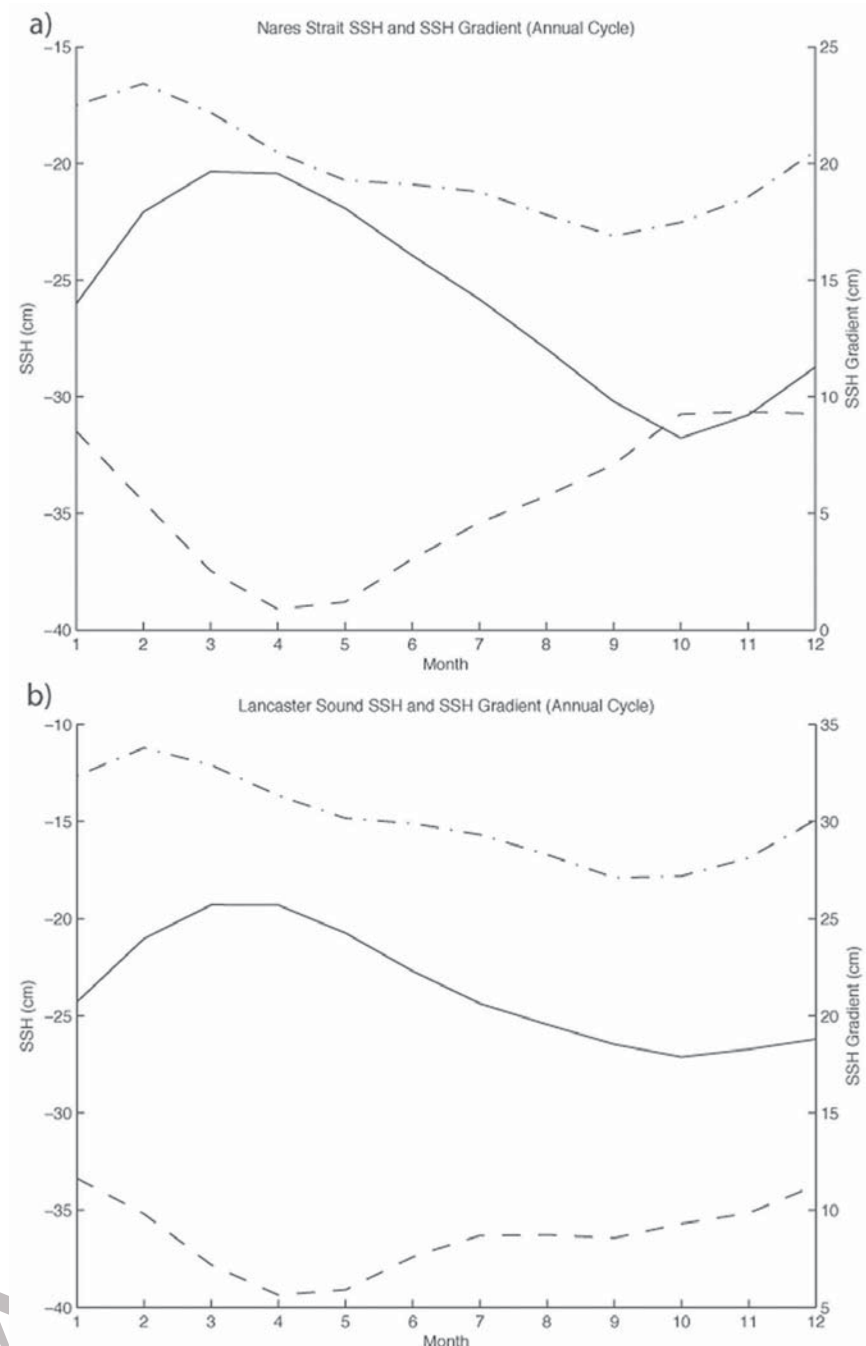

Figure 14. Annual cycle of SSH (cm) and SSH gradient (cm): (a) dash-dot line, Lincoln Sea SSH; dashed line, Smith Sound SSH; solid line, SSH gradient along Nares Strait; (b) dash-dot line, Queen Elizabeth Islands SSH; dashed line, Baffin Bay SSH; solid line, SSH gradient along Lancaster Sound.

similar to findings of *Houssais and Herbaut* [2011] (who used annual instead of monthly mean values). For Lancaster Sound, the negative downstream SSH anomalies in western Baffin Bay correlated better with the SSH gradient anomalies than the SSH anomalies upstream in the Queen Elizabeth Islands (QEI). These findings confirm what *Kliem and Greenberg* [2003] had proposed: that the gradient is just as much if not more controlled by the sea surface drop in Baffin Bay as by an increase in the Arctic Ocean.

[44] For Lancaster Sound, the upstream end of the SSH gradient is traditionally considered to lie at the edge of the Beaufort Sea near McClure Strait. However, volume flux anomalies were better correlated with the SSH gradient measured from above the QEI to western Baffin Bay (R = 0.85) as opposed to being measured from the Beaufort Gyre to western Baffin Bay (R = 0.48). Cross sections of flow through western Lancaster Sound (see Figure 8) show the summertime maximum velocities are near the surface toward the southern side of the strait (consistent with wind-forcing),

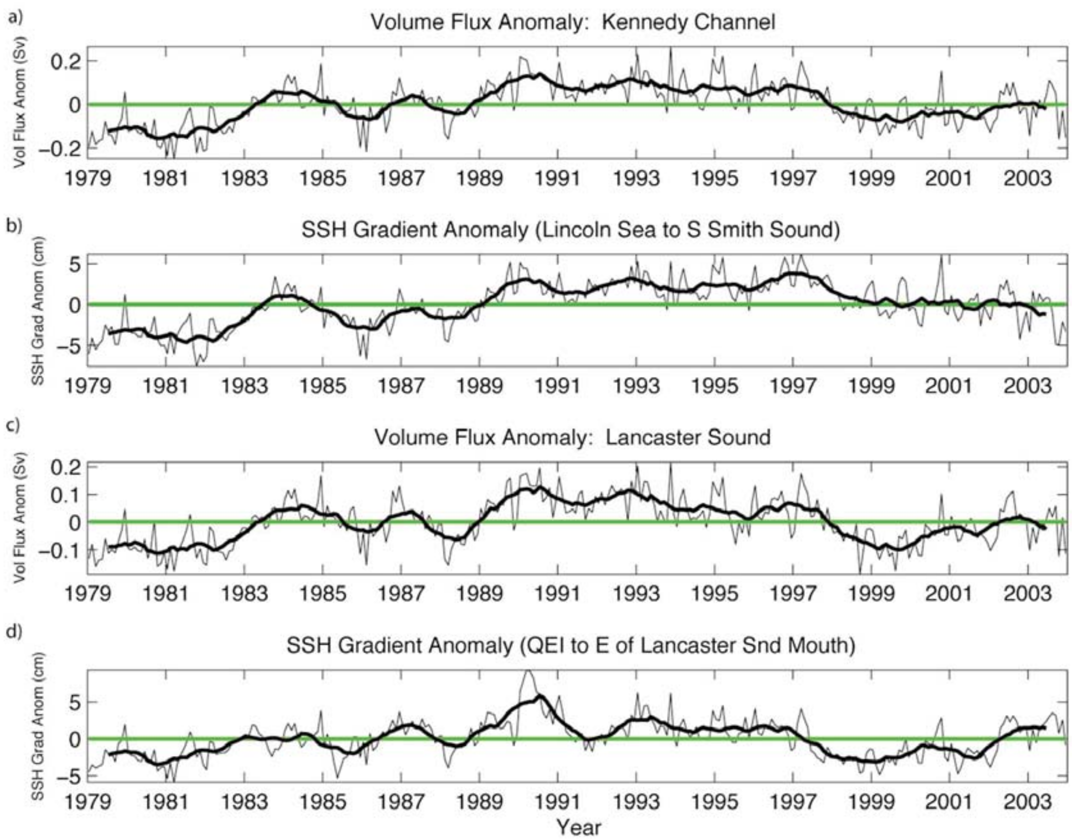

Figure 15. Monthly (a) volume flux anomalies through Nares Strait, (b) SSH gradient (from the Lincoln Sea to Baffin Bay), (c) volume flux anomalies through Lancaster Sound, and (d) SSH gradient (from the Queen Elizabeth Islands to Baffin bay). Thick black line is 13-month running mean.

whereas the wintertime maximum velocities are more evenly distributed over the water column (consistent with more of a barotropic response to a large scale gradient) on the northern side of the strait (consistent with control by the input from the QEI region vice Beaufort Gyre). *Houssais and Herbaut* [2011] showed that the flow (year to year) through Lancaster Sound was largely controlled by the SSH gradient across McClure Strait (which itself was linked to wind stress curl in the western Arctic). Here, we show that the along strait SSH gradient is dominant (like in the Nares Strait case) and that its endpoint lies to the north instead of to the west.

[45] The upstream ends of the calculated SSH gradients were located in the Arctic Ocean. As such, those SSH's and SSH anomalies were the product of a complex circulation north of the CAA. There the currents are highly variable along the slope, shelf, and coast, as well as possibly being affected by the major large-scale Arctic Ocean circulation patterns. The SSH and SSH anomaly time series' were correlated with the AO and NAO on monthly, seasonal, and annual time scales but only a small portion of variance could be explained (~10%). The Arctic dipole anomaly [*Wu et al.*, 2006, 2008] does not appear to explain the time series variability either. Furthermore, there is a lack of observational data in this region leaving its circulation and hydrography largely unknown. However, examination of the downstream ends of the SSH gradients (locations in northern Baffin Bay) sheds light on the volume fluxes through the major CAA passages.

9.5. Baffin Bay

[46] Baffin Bay is located between Baffin Island and Greenland and opens to the Labrador Sea in the south (Figure 16). It is about 1000 km long, 400 km wide and its depths exceed 2300 m. It is the collection point for CAA outflow as it continues enroute to the Labrador Sea. It receives inputs from Nares Strait, Jones Sound, and Lancaster Sound. It also receives volume input from the West Greenland Current (WGC) flowing north through eastern Davis Strait and loses volume as the Baffin Island Current flows southwards along western side of Davis Strait. This current system gives Baffin Bay a cyclonic circulation regime. The waters in the Baffin Island Current are mostly of Arctic origin and cold and fresh while those flowing in the opposite direction in the WGC are warmer and saltier due to the Irminger Water it carries. Deep flow between Baffin Bay and the Labrador Sea is prevented by a ~670 m deep sill in Davis Strait.

[47] Sea ice coverage is highly variable, with the bay covered in the winter by first year ice (Figure 9a) that almost completely disappears in summer (Figure 9b). Winter ice covers all of Baffin Bay except the region in eastern Davis Strait that receives heat from the WGC [*Tang et al.*, 2004]. The model does reproduce this feature, as well as the

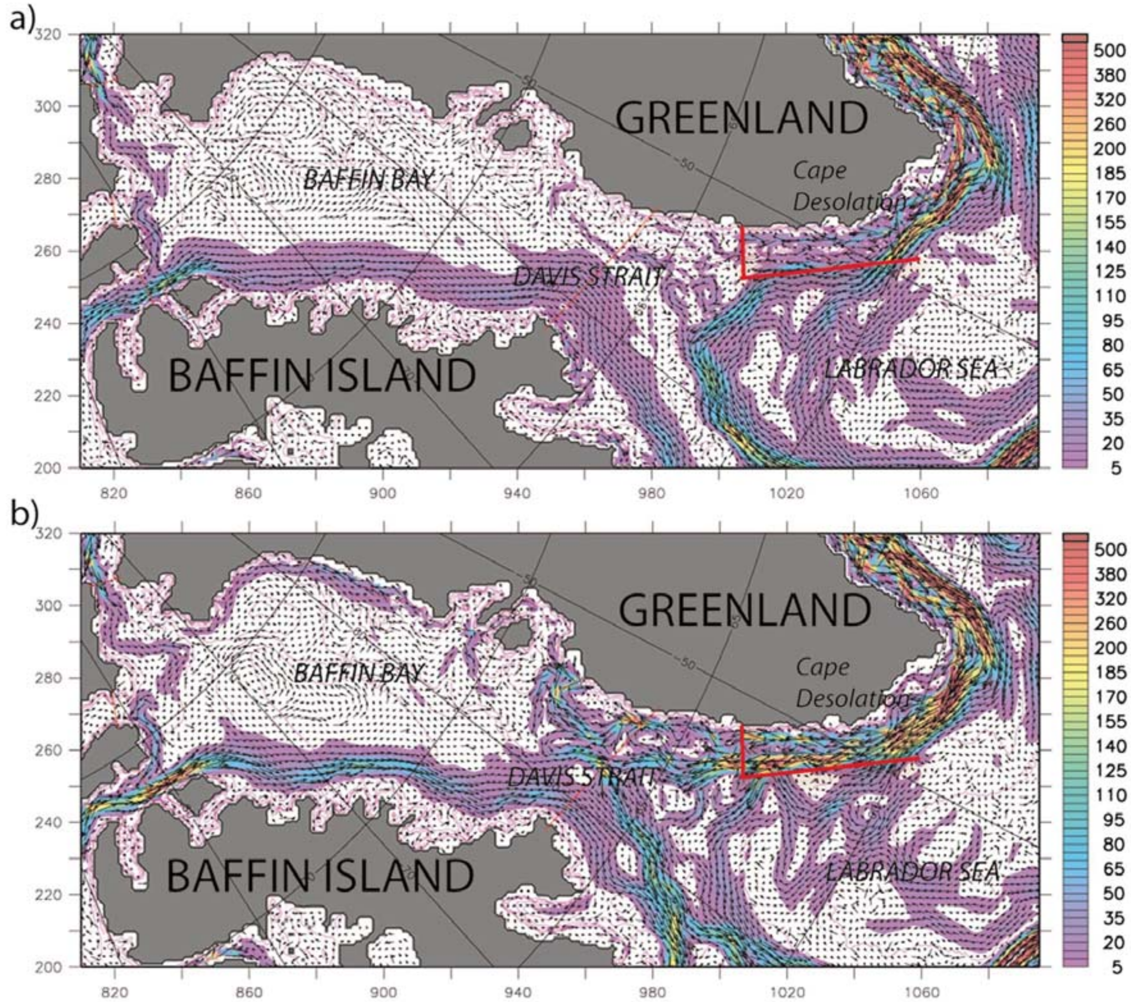

Figure 16. Baffin Bay 0–122 m 26-year mean velocity (vectors) and TKE (shading): (a) March and (b) September.

previously mentioned North Water Polynya which occurs in the north near Smith Sound [*Barber et al.*, 2001]. Observations [*Tang et al.*, 2004] show that a small amount of ice does survive the summer melt. Estimates of that minimum ice area correspond well with our model results [see *Tang et al.*, 2004, Figure 6].

[48] Baffin Bay's circulation changes strength seasonally. When the bay is ice covered in winter the ocean is insulated from much of the wind effects and currents are weaker (Figure 16a). In summer the ice has retreated and the ocean is exposed to the atmosphere and the currents are stronger (Figure 16b). These findings are similar to the observations of *Tang et al.* [2004] who found weaker currents in winter/spring and stronger currents in summer/fall. The modeled currents in eastern (especially northeastern) Baffin Bay are much stronger during the summer open water period, a finding consistent with the model experiments of *Dunlap and Tang* [2006], who showed that the strongest effects of wind-forcing (for September only) were confined to eastern Baffin Bay, (particularly to the northeast). The long-term model volume fluxes into and out of Baffin Bay balance, as expected by continuity. The modeled freshwater fluxes (combined liquid and solid) into and out of Baffin Bay are nearly balanced, with more freshwater going out than coming in being due to net precipitation ($\sim$7 mSv) accounted for in the model by restoring.

[49] Based on the model-derived annual cycle, Baffin Bay's sea surface drops from February to April and then rises back up for the rest of the year. The effect is most evident on the eastern side of the bay. This is not just a redistribution of mass across the bay: the actual volume of Baffin Bay fluctuates over this cycle. The Baffin Bay volume anomaly leads both the Lancaster Sound and Nares Strait volume flux anomalies by one month with correlations of $R = -0.73$ (for each) suggesting that the volume decrease which controls SSH in Baffin Bay drives increased fluxes through the CAA. Moreover, the decreases in Baffin Bay SSH and volume coincide with a decrease in the northward volume transport by the West Greenland Current (WGC) into Baffin Bay from the south (Figure 17). This differs from the model findings of *Houssais and Herbaut* [2011], who determined that changes in Baffin Bay SSH were remotely forced by air-sea heat flux in the Labrador Sea. Our model suggests that volume flux of the WGC drives Baffin Bay SSH. In fact, the flow along the western Greenland shelf north of Davis Strait actually turns southwards from

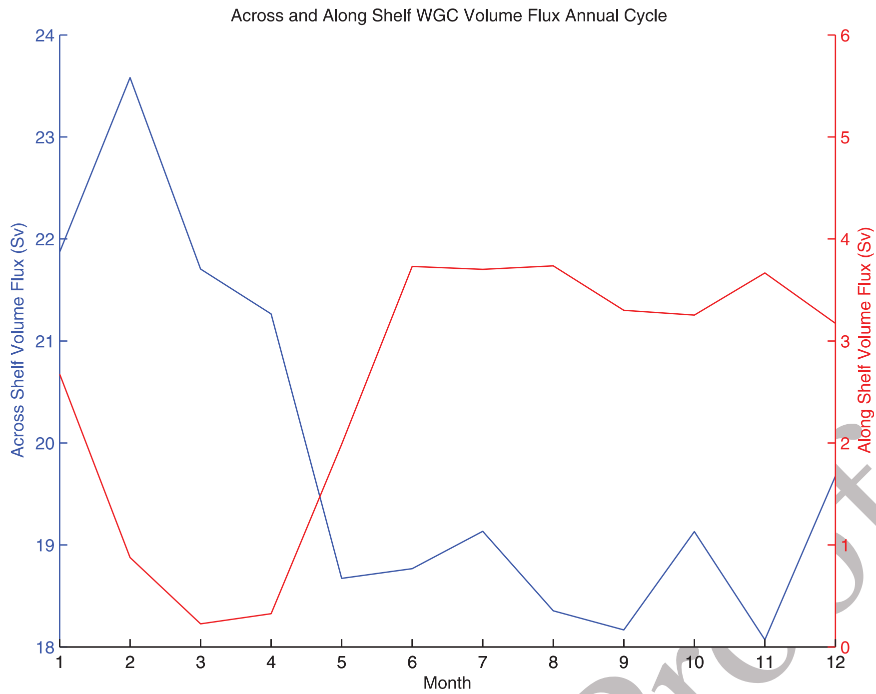

Figure 17. Western Greenland net annual volume flux cycles (blue, across shelf; red, along shelf (downstream of the across shelf region)).

February to April (some weak northbound flow does continue on the eastern side of Davis Strait but it is dominated by the southbound flow in the net sense). Using a mooring in eastern Davis Strait, *Tang et al.* [2004] observed that the northward current was strongest in fall and weakest in winter, sometimes even changing direction to indicate southward flow. *Rykova et al.* [2010] determined the WGC to be widest and fastest in November and slowest in April/March. Both of these studies are consistent with our simulated seasonal variability of flow in eastern Davis Strait.

9.6. The West Greenland Current Near Cape Desolation

[50] The possible cause of variability in the northward flow can be traced all the way back to Cape Desolation in the south. Near Cape Desolation, the WGC fractures into three branches with one continuing north along the West Greenland coast and the others following the bathymetry to the west around the northern rim of the Labrador basin [*Cuny et al.*, 2002]. Previous comparison of results from this model with available data show similar spatial distribution and magnitude of eddy kinetic energy [*Maslowski et al.*, 2008] suggesting agreement not just with the linear branch of the current but also with the magnitude and frequency of eddies separating from the WGC. This is in fact a site of observed eddy production [*Prater*, 2002; *Lilly et al.*, 2003; *Hatun*, 2007]. Eddies enter the central Labrador Sea along the recirculating branches and are thought to play significant roles in the preconditioning, deep convection, and restratification processes [*Katsman et al.*, 2004; *Chanut et al.*, 2008; *Rykova et al.*, 2010]. In a modeling study, *Eden and Boning* [2002] found that eddies shed near Cape Desolation were formed by instability in the WGC southwards of that location. The instability and eddy generation was seasonal, peaking in January/February/March, consistent with the time period when recirculaton (offshore branching and eddy flux into the Labrador Sea interior) is strongest in our model. Over the annual cycle, the model shows that as the across shelf volume flux peaks the northward volume transport in the WGC decreases (Figure 17). Conversely, when the across shelf volume flux is at its minimum the northward flux builds up again. There is very little correlation in volume flux anomalies (measured along the shelf) between successive locations while moving northward up the western coast of Greenland. Most of the variance in the volume flux anomaly signal can be tracked moving across the shelf into the interior of the Labrador Sea rather than continuing northward along Greenland. The variable dynamics that control the volume directed offshore make it impossible for volume flux anomalies to propagate northward with their overall signal intact. *Dunlap and Tang* [2006] used a model to show that increasing the volume flux south of Greenland (rounding Cape Farewell) "mostly affects the part of the WGC that branches westward at about 64 N." Possibly related, *Houghton and Visbeck* [2002] showed that freshwater anomalies observed near Cape Farewell are much different than those moving northward through eastern Davis Strait. As the anomalies are continually removed, the annual cycle is all that is left for comparison. The annual peak of cross shelf flow corresponds to a slack period in the northward flow. This contributes to the volume and SSH variation in Baffin Bay.

[51] Of particular interest is what causes the recirculation branches to leave the west Greenland shelf. Plots of wind stress and wind stress curl show that when the most recirculation is occurring (January/February/March), the winds exert a cyclonic torque on the upper ocean over the region where they move offshore (Figure 18a). This area is ice free

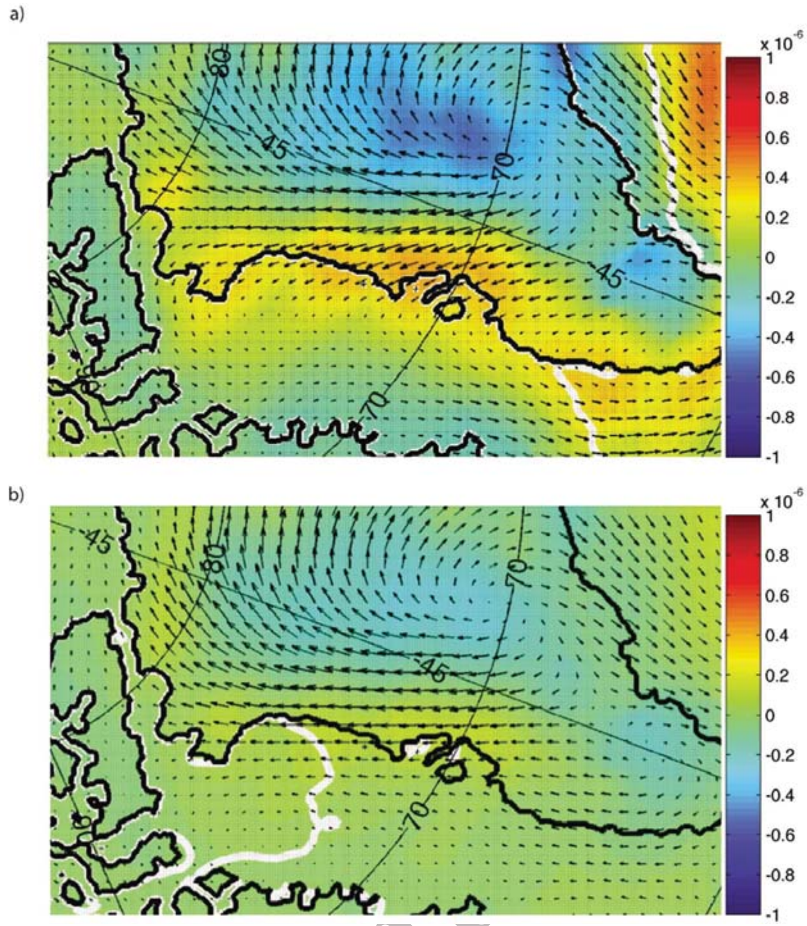

Figure 18. Wind stress (vectors), wind stress curl (N m^{-3}) (shading) and 30% ice concentration (white contour) for (a) March and (b) August.

in the model and observations, allowing the wind to act on the open water. *Eden and Boning* [2002] found that wind stress does play a role on the instability of the WGC and eddy formation during this season. There is cyclonic torque exerted on the surface in other regions along the west Greenland shelf and eastern Baffin Bay. However, those areas are covered by smooth first year ice at the time, effectively de-coupling the ocean from the atmosphere. Later, after the ice has receded, the winds are favorable to flow along the western Greenland coast (Figure 18b), and the flow does increase there (Figures 16b and 17).

[52] However, it is difficult to completely attribute the SSH drop to any one event. Other factors possibly causing SSH to drop in northeast Baffin Bay are local cooling of the water and the input of brine as a result of ice formation, both of which increase density and lower SSH. In fact, the time series of ice volume anomalies in Baffin Bay correlates with the volume anomalies in Baffin Bay at R = -0.5 at zero lag. Furthermore, during the time of the lowest SSH, the area with the lowest SSH experiences the highest sea surface salinity in any region of Baffin Bay over the entire annual cycle.

9.7. Davis Strait SSH Gradients and Outflow

[53] After CAA outflow moves into Baffin Bay, it is exported southward to the Labrador Sea via Davis Strait. There is an across strait SSH gradient of approximately 10 cm across Davis Strait, with the western side of the strait sitting higher than the eastern side. The western side of the strait changes little whereas the eastern side exhibits large variability. Using the annual cycle of SSH gradients calculated between northern Baffin Bay and various points along the Davis Strait section (Figure 19), it becomes evident that the SSH gradients are most variable on the eastern side of Davis Strait. There, the gradient goes positive and negative (Figure 19c). It is positive (oriented with northern Baffin Bay higher than eastern Davis Strait) in the winter months during which time the volume transport is weakest in the WGC, allowing the maximum net volume outflow from Davis Strait south to the Labrador Sea. During the late summer/fall, the SSH gradient has switched signs (with eastern Davis Strait higher than northern Baffin Bay), which coincides with the peak volume inflow from the WGC, resulting in the minimum net outflow from Davis Strait. Thus, sign changes in this gradient are associated with flood and ebb of WGC into and out of Baffin Bay.

[54] The time series of SSH gradient anomalies measured from northern Baffin Bay to various points along the Davis Strait section are presented in Figure 20. Numerous combinations of points between northern Baffin Bay and across the width of Davis Strait were considered and a few are shown

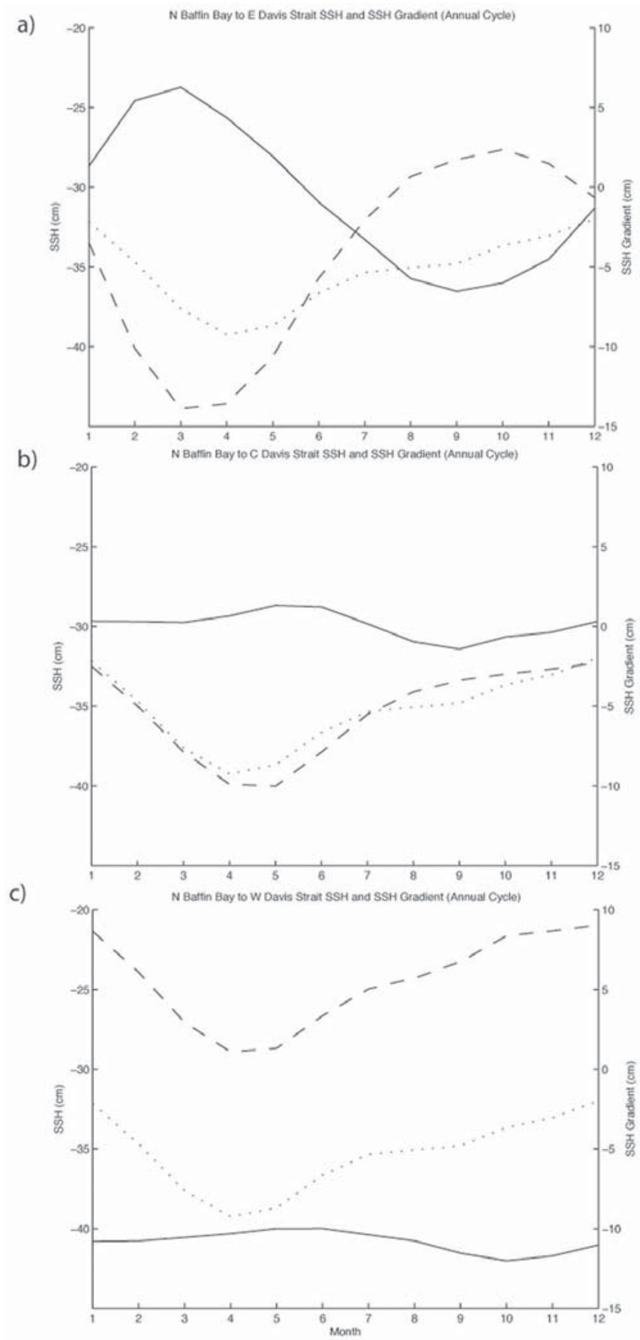

Figure 19. Annual cycle of SSH (cm) and SSH gradient (cm). Dashed line, N Baffin Bay SSH; dotted line, 3 SSH locations in Davis Strait: (a) eastern Davis Strait, (b) central Davis Strait, and (c) western Davis Strait; solid line, SSH gradient between them.

here for illustration. As one goes from west to east, the time series of SSH gradient anomalies become increasingly similar in shape to the time series of net volume flux anomalies through Davis Strait (Figure 20) with correlations at locations in western Davis Strait, central Davis Strait, and eastern Davis Strait of R = 0.53, 0.61, and 0.86 respectively. Variability of SSH gradient anomalies are the least correlated with net volume flux anomalies since 2000, when the volume flux anomaly in Davis Strait goes to zero while the SSH gradient anomalies continue decreasing. This is opposite of the trend in the time series before 2000 and might be a results of multiple factors (e.g., changes in SSH gradient across the strait, decrease of SSH in northern Baffin Bay, delayed response between SSH and volume flux, or else) however further investigation of such a behavior is beyond the scope of this paper.

[55] Yet, to monitor the flow through the CAA one could possibly observe the SSH gradient from northern Baffin Bay to eastern Davis Strait. Furthermore, to estimate the net volume export into the Labrador Sea one could even just monitor the SSH in eastern Davis Strait. The time series of SSH anomaly in eastern Davis Strait correlated with net volume flux anomalies through Davis Strait into the Labrador Sea yields a value of R = −0.83.

[56] The southward movement of freshwater through Davis Strait was examined. The best correlation (R = 0.52) between Davis Strait net freshwater flux (liquid) anomalies and Baffin Bay N-S SSH gradient anomalies occurred when the downstream endpoint of the gradient was in eastern Davis Strait, just as was the case for volume flux anomalies. When considering ice fluxes as well, the combined freshwater flux anomalies correlated even better with the N-S Baffin Bay SSH gradient anomalies (R = 0.65). This increase in correlation does not suggest that the SSH gradient anomalies push ice through Davis Strait, but rather that anomalies in winds which may cause anomalies in the gradient may also drive an increase in the ice flux. For example, an anomalous northerly wind could drive more recirculation offshore from the Greenland shelf, reduce SSH there, and cause an increased SSH gradient. That same northerly wind could also drive extra ice southwards through Davis Strait.

[57] What drove the SSH gradient (between northern Baffin Bay and eastern Davis Strait) anomalies and Davis Strait net volume flux anomalies to such a high values in early mid 1990s is still an open question. This was a time of a highly positive Arctic Oscillation (AO) index, which yields more cyclonic conditions in the Arctic that would favor flow through the CAA. However, correlation of the volume flux anomalies with AO and the North Atlantic Oscillation (NAO) indices explain little of the variance (~20% and ~15% respectively). Perhaps this was due to the correlations being based on the entire 26-year time series of monthly values, allowing other variability to overshadow better agreement over the shorter periods. This study has shown the importance of control by the West Greenland Current, suggesting the cause could be traced back to that region.

[58] In summary, variations in the northward flow in eastern Davis Strait provide a significant control on the flow moving from the Arctic Ocean through the CAA to Baffin Bay. *Dunlap and Tang* [2006] also found a connection between CAA outflow and the flow strength in eastern Davis Strait but determined the opposite: flow through the CAA regulated the northbound inflow to Baffin Bay. Our model has demonstrated the opposite, where flow in eastern Davis Strait regulates CAA outflow. However, their solution was based solely on September simulation and many of the details presented here (i.e., seasonal cycles in WGC and recirculating branches into the Labrador Sea, etc.) would not

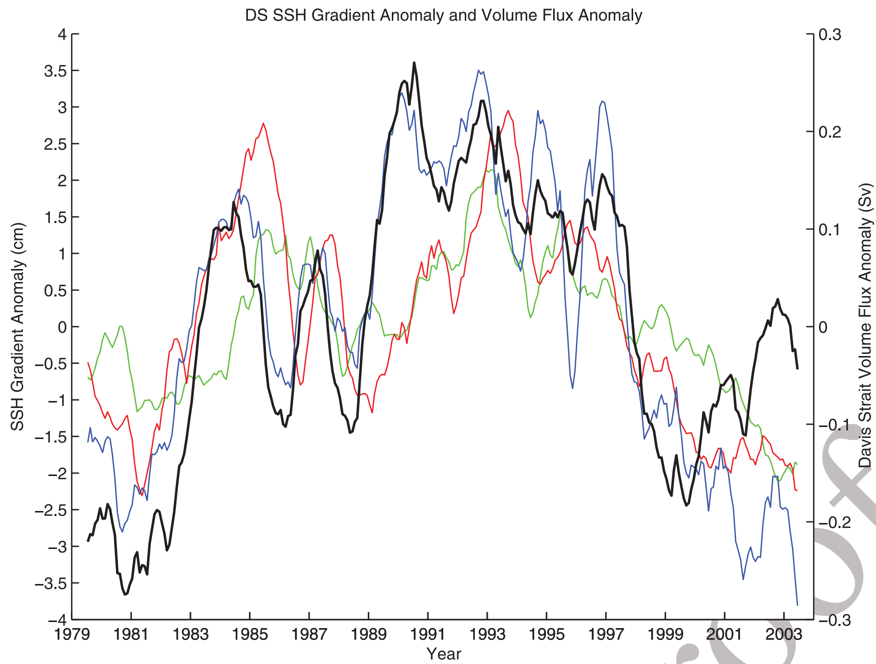

Figure 20. SSH gradient anomalies (13-month running mean) measured from northern Baffin Bay to several locations along the Davis Strait section. Green, western Davis Strait; red, central Davis Strait; blue, eastern Davis Strait; black, Davis Strait net volume flux anomaly (13-month running mean).

have been available to resolve the cause/effect nature of the processes.

10. Summary

[59] This study determined the 1979–2004 volume and freshwater fluxes through the Canadian Arctic Archipelago using a high-resolution (~9 km) numerical model, compared them with limited observational estimates, and briefly examined their controls. It was determined that the 26-year mean volume and freshwater fluxes through Nares Strait were 0.77 Sv ± 0.17 Sv and 10.38 mSv ± 1.67 mSv respectively, while those through Lancaster Sound amounted to 0.76 Sv ± 0.12 Sv and 48.45 mSv ± 7.83 mSv respectively. Thus the volume fluxes through the two main passages were nearly the same but the freshwater flux was much greater for Lancaster Sound. The 26-year mean volume and freshwater fluxes through Davis Strait were 1.55 Sv ± 0.29 Sv and 62.66 mSv ± 11.67 mSv.

[60] Additional freshwater flux into the Labrador Sea comes from Hudson Bay via Hudson Strait as well as via the East/West Greenland currents through the Fram/Denmark Strait pathway. While the net volume flux out of Hudson Bay is minimal (0.17 Sv) its modeled freshwater flux is significant (10.25 mSv or ~14%) relative to that out of Baffin Bay. The modeled freshwater flux through Hudson Strait represents only 17–36% of observational estimates, implying a large contribution of river runoff into Hudson Bay, which is not fully accounted in the model via the surface salinity restoring. This fact points to even a larger role of Hudson Bay as a source of freshwater to the Labrador Sea.

[61] In contrast, compared to the combined mean freshwater flux into the Labrador Sea through Davis and Hudson straits (85.73 mSv), the modeled Fram/Denmark strait branch contribution within WGC passed Cape Farewell is minimal (1.7 mSv or ~2%) as the majority (~97%) of the freshwater signal through Fram Strait is subject to mixing with high salinity Atlantic water along EGC in the Greenland, Iceland, and Irminger seas. Use of higher reference salinity than 34.8 yields larger magnitude of freshwater fluxes (not shown) but this is because it accounts for diffused freshwater signal above salinity of 34.8, which reduces its potential impact on the dynamics of the upper Labrador Sea.

[62] Volume flux anomalies through Nares Strait and Lancaster Sound were controlled by the SSH gradient anomalies along the straits and FW anomalies were highly correlated with the volume anomalies. At least half of the variance in the time series of SSH gradient anomaly was due to SSH anomalies in northern Baffin Bay. The West Greenland Current exhibits seasonality, with cross shelf flow (into the Labrador Sea) peaking in January/February/March, causing reduced northward flow across eastern Davis Strait. The decreased northward flow contributes to decreases in the volume and SSH in Baffin Bay. This maximizes the SSH gradients between the Arctic Ocean and Baffin Bay, leading to maximum volume fluxes through Nares Strait and Lancaster Sound. The net flow through Davis Strait toward the Labrador Sea is at a maximum in winter when the WGC is at its weakest and volume anomalies are most correlated with the SSH gradient anomalies measured from northern Baffin Bay to eastern Davis Strait.

[63] When compared to available observations, the model does provide similar volume and freshwater fluxes, as well as ice thickness and concentration in the CAA. However, further improvements are still possible and required to minimize model limitations due to the lack of high resolution

atmospheric forcing (especially the effects of local topography), the representation of river runoff into Hudson Bay and coastal buoyancy currents, low mobility of modeled ice, and incomplete depiction of ice arching. Additionally, model bathymetry and horizontal resolution are critical because they play significant roles in representing passages within the CAA and determining where (near Cape Desolation) the recirculating branches separate from the western Greenland shelf into the Labrador Sea interior. The recirculation is also associated with the formation of eddies [*Katsman et al.*, 2004; *Chanut et al.*, 2008], which again are resolution dependent. This regulates the northward flow through Davis Strait and contributes to volume and SSH variations in Baffin Bay, the along strait SSH gradients and the flow through the CAA. Additional studies devoted solely to the circulation and dynamics of Baffin Bay and the WGC current system should yield even more insight into mechanisms controlling CAA throughput. However, increased model grid cell resolution, improved sea ice and ocean models and more realistic atmospheric forcing are required. As future freshwater fluxes through the CAA are expected to increase with climatic implications, it is imperative that models are capable of realistic depiction of the two pathways of freshwater export from the Arctic Ocean. Finally, more data for model validation is needed in order to advance understanding of the role of freshwater sources in the Labrador Sea and to improve their representation in global climate models.

[64] **Acknowledgments.** The ARCSS Program of the National Science Foundation, the Climate Change Prediction Program of the Department of Energy, and the Office of Naval Research provided funding for the development and integration of the coupled ice-ocean model. We would like to thank the Commander Naval Meteorology and Oceanography Command and the Naval Postgraduate School for the opportunity to pursue this project as part of a PhD dissertation (T.M.). We also thank Jaclyn Clement Kinney for her help with model data, processing programs, and overall assistance. The Arctic Region Supercomputer Center (ARSC), Fairbanks, Alaska, through the Department of Defense High Performance Computer Modernization Program (DOD/HPCMP), provided computer resources. The Arctic Ocean Modeling Intercomparison Project (AOMIP) provided (T.M.) travel assistance to the 2010 school and meeting, facilitating contacts, feedback, and the exchange of ideas reflected in this paper.

References

Agnew, T., A. Lambe, and D. Long (2008), Estimating sea ice area flux across the Canadian Arctic Archipelago using enhanced AMSR-E, *J. Geophys. Res.*, *113*, C10011, doi:10.1029/2007JC004582.

Barber, D. G., J. M. Hanesiak, W. Chan, and J. Piwowar (2001), Sea-ice and meteorological conditions in northern Baffin Bay and the North Water polynya between 1979 and 1996, *Atmos. Ocean*, *39*(3), 343–359.

Belkin, I. M., S. Levitus, J. Antonov, and S. Malmberg (1998), "Great Salinity Anomalies" in the North Atlantic, *Prog. Oceanogr.*, *41*, 1–68.

Broecker, W. (1991), The great ocean conveyor, *Oceanography*, *4*, 79–89.

Chanut, J., B. Barnier, W. Large, L. Debreu, T. Penduff, J. M. Molines, and P. Mathiot (2008), Mesoscale eddies in the Labrador Sea and their contribution to convection and restratification, *J. Phys. Oceanogr.*, *38*, 1617–1643.

Cheng, W., and P. B. Rhines (2004), Response of overturning circulation to high-latitude fresh-water perturbations in the North Atlantic, *Clim. Dyn.*, *22*, 359–372.

Cuny, J., P. Rhines, S. Niiler, and S. Bacon (2002), Labrador Sea boundary currents and the fate of the Irminger Sea Water, *J. Phys. Oceanogr.*, *32*, 627–647.

Cuny, J., P. B. Rhines, and R. Kwok (2005), Davis Strait volume, freshwater and heat fluxes, *Deep Sea Res., Part I*, *52*, 519–542.

Curry, B., C. M. Lee, and B. Petrie (2011), Volume, freshwater, and heat fluxes through Davis Strait 2004–2005, *J. Phys. Oceanogr.*, *41*, 429–436.

de Steur, L., E. Hansen, R. Gerdes, M. Karcher, E. Fahrbach, and J. Holfort (2009), Freshwater fluxes in the East Greenland Current: A decade of observations, *Geophys. Res. Lett.*, *36*, L23611, doi:10.1029/2009GL041278.

Dickson, R., S. Dye, M. Karcher, J. Meincke, B. Rudels, and I. Yashayaev (2007), Current estimates of freshwater flux through arctic and subarctic seas, *Prog. Oceanogr.*, *73*, 210–230.

Dunbar, M. (1973), Ice regime and ice transport in Nares Strait, *Arctic*, *26*, 282–291.

Dunlap, E., and C. C. L. Tang (2006), Modelling the mean circulation of Baffin Bay, *Atmos. Ocean*, *44*(1), 99–110.

Eden, C., and C. Boning (2002), Sources of eddy kinetic energy in the Labrador Sea, *J. Phys. Oceanogr.*, *32*, 3346–3363.

Fissel, D. B., D. D. Lemon, and J. R. Birch (1982), Major features of the summer near-surface circulation of western Baffin Bay, 1978 and 1979, *Arctic*, *35*, 180–200.

Goosse, H., T. Fichefet, and J. M. Campin (1997), The effects of the water flow through the Canadian Archipelago in a global ice-ocean model, *Geophys. Res. Lett.*, *24*, 1507–1510.

Hakkinen, S. (1999), A simulation of thermohaline effects of a Great Salinity Anomaly, *J. Clim.*, *12*, 1781–1795.

Hatun, H. (2007), Buoyant eddies entering the Labrador Sea observed with gliders and altimetry, *J. Phys. Oceanogr.*, *37*, 2838–2854.

Hibler, W. D., III (1979), A dynamic thermodynamic sea ice model, *J. Phys. Oceanogr.*, *9*, 815–846.

Houghton, R. W., and M. H. Visbeck (2002), Quasi-decadal salinity fluctuations in the Labrador, *J. Phys. Oceanogr.*, *32*, 687–701.

Houssais, M. N., and C. Herbaut (2011), Atmospheric forcing on the Canadian Arctic Archipelago freshwater outflow and implications for the Labrador Sea variability, *J. Geophys. Res.*, *116*, C00D02, doi:10.1029/2010JC006323.

Hu, A., B. L. Otto-Bliesner, G. A. Meehl, W. Han, C. Morrill, E. C. Brady, and B. Briegleb (2008), Response of thermohaline circulation to freshwater forcing under present-day and LGM conditions, *J. Clim.*, *21*, 2239–2258.

Jahn, A., L. B. Tremblay, R. Newton, M. M. Holland, L. A. Mysak, and I. A. Dmitrenko (2010), A tracer study of the Arctic Ocean's liquid freshwater export variability, *J. Geophys. Res.*, *115*, C07015, doi:10.1029/2009JC005873.

Jakobsson, M., N. Cherkis, J. Woodward, R. Macnab, and B. Coakley (2000), New grid of Arctic bathymetry aids scientists and mapmakers, *Eos Trans. AGU*, *81*(9), 89.

Joyce, T. M., and A. Proshutinsky (2007), Greenland's Island Rule and the Arctic Ocean circulation, *J. Mar. Res.*, *65*, 639–653.

Jungclaus, J. H., H. Haak, M. Latif, and U. Mikolajewicz (2005), Arctic–North Atlantic interactions and multidecadal variability of the meridional overturning circulation, *J. Clim.*, *18*, 4013–4031.

Katsman, C. A., M. A. Spall, and R. S. Pickart (2004), Boundary current eddies and their role in the restratrication of the Labrador Sea, *J. Phys. Oceanogr.*, *34*, 1967–1983.

Kliem, N., and D. A. Greenberg (2003), Diagnostic simulations of the summer circulation in the Canadian Arctic Archipelago, *Atmos. Ocean*, *41*(4), 273–289.

Koberle, C., and R. Gerdes (2007), Simulated variability of the Arctic Ocean freshwater balance 1948–2001, *J. Phys. Oceanogr.*, *37*, 1628–1644.

Koenigk, T., U. Mikolajewicz, H. Haak, and J. Jungclaus (2007), Arctic freshwater export in the 20th and 21st centuries, *J. Geophys. Res.*, *112*, G04S41, doi:10.1029/2006JG000274.

Komuro, Y., and H. Hasumi (2005), Intensification of the Atlantic Deep Circulation by the Canadian Archipelago Throughflow, *J. Phys. Oceanogr.*, *35*, 775–789.

Kwok, R. (2005), Variability of Nares Strait ice flux, *Geophys. Res. Lett.*, *32*, L24502, doi:10.1029/2005GL024768.

Kwok, R. (2006), Exchange of sea ice between the Arctic Ocean and the Canadian Arctic Archipelago, *Geophys. Res. Lett.*, *33*, L16501, doi:10.1029/2006GL027094.

Kwok, R. (2007), Baffin Bay ice drift and export: 2002–2007, *Geophys. Res. Lett.*, *34*, L19501, doi:10.1029/2007GL031204.

Kwok, R., G. F. Cunningham, and S. S. Pang (2004), Fram Strait sea ice outflow, *J. Geophys. Res.*, *109*, C01009, doi:10.1029/2003JC001785.

Kwok, R., L. T. Pedersen, P. Gudmandsen, and S. S. Pang (2010), Large sea ice outflow into Nares Strait in 2007, *Geophys. Res. Lett.*, *37*, L03502, doi:10.1029/2009GL041872.

Lietaer, O., T. Fichefet, and V. Legat (2008), The effects of resolving the Canadian Arctic Archipelago in a finite element sea ice model, *Ocean Modell.*, *24*, 140–152.

Lilly, J. M., P. B. Rhines, F. Schott, K. Lavender, J. Lazier, U. Send, and E. d'Asaro (2003), Observations of the Labrador Sea eddy field, *Prog. Oceanogr.*, *59*, 75–176.

Marshall, J., and F. Schott (1999), Open-ocean convection: Observations, theory, and models, *Rev. Geophys.*, *37*, 1–64.

Maslowski, W., and W. H. Lipscomb (2003), High-resolution simulations of Arctic sea ice during 1979–1993, *Polar Res.*, *22*, 67–74.

Maslowski, W., D. Marble, W. Walczowski, U. Schauer, J. L. Clement, and A. J. Semtner (2004), On climatological mass, heat, and salt transports through the Barents Sea and Fram Strait from a pan-Arctic coupled ice-ocean model simulation, *J. Geophys. Res.*, *109*, C03032, doi:10.1029/2001JC001039.

Maslowski, W., J. C. Kinney, and J. Jakacki (2007), Toward prediction of environmental arctic change, *Comput. Sci. Eng.*, *9*(6), 29–34.

Maslowski, W., J. C. Kinney, D. Marble, and J. Jakacki (2008), Towards eddy-resolving models of the Arctic Ocean, in *Ocean Modeling in an Eddying Regime*, *Geophys. Monogr. Ser.*, vol. 177, edited by M. W. Hecht and H. Hasumi, pp. 241–264, AGU, Washington, D. C.

McGeehan, T. P., and W. Maslowski (2011), Impact of shelf-basin freshwater transport on deep convection in the western Labrador Sea, *J. Phys. Oceanogr.*, *41*, 2187–2210, doi:10.1175/JPO-D-11-01.1.

Melling, H., T. A. Agnew, K. K. Falkner, D. A. Greenberg, C. M. Lee, A. Munchow, B. Petrie, S. J. Prinsenberg, R. M. Samelson, and R. A. Woodgate (2008), Fresh-water fluxes via Pacific and Arctic outflows across the Canadian polar shelf, in *Arctic-Subarctic Ocean Fluxes*, edited by R. R. Dickson et al., pp. 193–247, Springer, Dordrecht, Netherlands.

Munchow, A., and H. Melling (2008), Ocean current observations from Nares Strait to the west of Greenland: Interannual to tidal variability and forcing, *J. Mar. Res.*, *66*, 801–833.

Munchow, A., H. Melling, and K. K. Faulkner (2006), An observational estimate of volume and freshwater flux leaving the Arctic Ocean through Nares Strait, *J. Phys. Oceanogr.*, *36*, 2025–2041.

Munchow, A., K. K. Faulkner, and H. Melling (2007), Spatial continuity of measured seawater and tracer fluxes through Nares Strait, a dynamically wide channel bordering the Canadian Archipelago, *J. Mar. Res.*, *65*, 759–788.

Peterson, I. K., S. J. Prinsenberg, J. Hamilton, and R. Pettipas (2008), Variability of oceanographic and ice properties of the Canadian Arctic Archipelago, paper presented at Annual Science Conference, Int. Counc. for the Explor. of the Sea, Halifax, N. S., Canada.

Prater, M. D. (2002), Eddies in the Labrador Sea as observed by profiling RAFOS floats and remote sensing, *J. Phys. Oceanogr.*, *32*, 411–427.

Prinsenberg, S. J., and E. B. Bennett (1987), Mixing and transports in barrow Strait, the central part of the Northwest Passage, *Cont. Shelf Res.*, *7*(8), 913–935.

Prinsenberg, S. J., and J. Hamilton (2005), Monitoring the volume, freshwater and heat fluxes passing through Lancaster Sound of the Canadian Arctic Archipelago, *Atmos. Ocean*, *43*(1), 1–22.

Prinsenberg, S., J. Hamilton, I. Peterson, and R. Pettipas (2009), Observing and interpreting the seasonal variability of the oceanographic fluxes passing through Lancaster Sound in the Canadian Arctic Archipelago, in *Influence of Climate Change on the Changing Arctic and Sub-Arctic Conditions*, edited by C. J. Nihoul and A. G. Kostianoy, pp. 125–143, Springer, Dordrecht, Netherlands.

Rykova, T., F. Straneo, J. M. Lilly, and I. Yashayev (2010), Irminger Current Anticyclones in the Labrador Sea observed in the hydrographic record, 1990–2004, *J. Mar. Res.*, *67*, 361–384.

Samelson, R. M., and P. L. Barbour (2008), Low-level jets, orographic effects, and extreme events in Nares Strait: A model-based mesoscale climatology, *Mon. Weather Rev.*, *136*, 4746–4759.

Samelson, R. M., T. Agnew, H. Melling, and A. Münchow (2006), Evidence for atmospheric control of sea-ice motion through Nares Strait, *Geophys. Res. Lett.*, *33*, L02506, doi:10.1029/2005GL025016.

Schauer, U., E. Fahrbach, S. Osterhus, and G. Rohardt (2004), Arctic warming through the Fram Strait: Oceanic heat transport from 3 years of measurements, *J. Geophys. Res.*, *109*, C06026, doi:10.1029/2003JC001823.

Smith, R., and P. Gent (2002), Reference manual for the Parallel Ocean Program (POP), *Unclassif. Rep. LA-UR-02-2484*, Los Alamos Natl. Lab., Los Alamos, N. M.

Steele, M., and W. Ermold (2007), Steric sea level change in the Northern Seas, *J. Clim.*, *20*, 403–417.

Steele, M., R. Morley, and W. Ermold (2000), PHC: A global ocean hydrography with a high quality Arctic Ocean, *J. Clim.*, *14*(9), 2079–2087.

Straneo, F., and F. Saucier (2008), The outflow from Hudson Strait and its contribution to the Labrador Current, *Deep Sea Res., Part I*, *55*, 926–946.

Sutherland, D. A., and R. S. Pickart (2008), The East Greenland Coastal Current: Structure, variability, and forcing, *Prog. Oceanogr.*, *78*, 58–77.

Tang, C. L., C. K. Ross, T. Yao, B. Petrie, B. M. DeTracey, and E. Dunlap (2004), The circulation, water masses and sea-ice of Baffin Bay, *Prog. Oceanogr.*, *63*, 183–228.

Vellinga, M., B. Dickson, and R. Curry (2008), The changing view on how freshwater impacts the Atlantic meridional overturning circulation, in *Arctic-Subarctic Ocean Fluxes*, edited by R. R. Dickson et al., pp. 289–313, Springer, Dordrecht, Netherlands.

Wadley, M. R., and G. R. Bigg (2002), Impact of flow through the Canadian Archipelago and Bering Strait on the North Atlantic and Arctic circulation: An ocean modeling study, *Q. J. R. Meteorol. Soc.*, *128*, 2187–2203.

Williams, K. (2004), The circulation and fluxes from the Arctic into the North Atlantic Ocean: 1979–2002 model results, MS thesis, 111 pp., Dep. of Oceanogr., Nav. Postgrad. Sch., Monterey, Calif.

Wu, B., J. Wang, and J. E. Walsh (2006), Dipole anomaly in the winter Arctic atmosphere and its association with sea ice motion, *J. Clim.*, *19*, 210–225.

Wu, B. Y., R. H. Zhang, and R. D'Arrigo (2008), Arctic dipole anomaly and summer rainfall in northeast China, *Chin. Sci. Bull.*, *53*(14), 2222–2229.

Zhang, J., and W. D. Hibler (1997), On an efficient numerical method for modeling sea ice dynamics, *J. Geophys. Res.*, *102*(C4), 8691–8702.

W. Maslowski and T. McGeehan, Department of Oceanography, Graduate School of Engineering and Applied Sciences, Naval Postgraduate School, Monterey, CA 93943, USA. (maslowsk@nps.edu; tpmcgeeh@nps.edu)